Nanoscale

REVIEW

View Article Online
View Journal | View Issue

Cite this: *Nanoscale*, 2021, **13**, 13574

Metal–metal bonds in polyoxometalate chemistry

Aleksandar Kondinski *†

Received 14th April 2021,
Accepted 8th July 2021

DOI: 10.1039/d1nr02357h

rsc.li/nanoscale

Half a century ago, F. Albert Cotton emphasized the relevance of metal–metal bonding in the constitution of cluster materials. Based on his description, nanoscale polyoxometalates (POMs) normally would not be regarded as cluster materials. One reason is that metal–metal bonding is typically associated with inorganic systems featuring metal centres in low oxidation states, a feature that is not common for POMs. However, over the past decades, there have been increasing reports on POMs integrating different types of metal–metal bonding. This article conceptualises and reviews the area of metal–metal bonded POMs, and their preparation and physicochemical properties. Attention is given to the changes in the electronic structure of POMs, the emergence of covalent dynamics and its impact on the development of applications in catalysis, nanoswitches, donor–acceptor systems, electron storage materials and nanoelectronics (*i.e.*, "POMtronics").

1. Introduction

Metals and metal oxides constitute the most common materials in Earth's crust. Since prehistoric times much of our technological and cultural progress has been closely related to the understanding of the properties of these materials and their processing.[1,2] The discovery of primitive metallurgy that led to the emergence of civilisations,[3] the discovery of metal nanoparticle and metal oxide pigments that transformed art,[4–6] and the enlightened discovery of oxygen by reducing mercury oxide and its role in setting the foundation of chemistry,[7–9] are some of the most quintessential examples that demonstrate this relationship. Over the past century, the meticulous engineering of metal–oxide semiconductors has enabled global computerisation,[10,11] while with approaching limits of Moore's law,[12,13] there are growing needs for the development of quantum computing and spintronic technologies, where again nanoscale metals and metal oxides are at the forefront of materials research.[14,15]

At the low nanoscale, metals and metal oxides can produce cluster-like materials that are discrete and atomistically precise. F. Albert Cotton was the pioneer who defined metal clusters and realised the role of metal–metal bonding in the constitution of these materials.[16] In this line, the discrete and atomistically precise metal oxides, polyoxometalates (POMs), did not exhibit metal–metal bonding in their constitution and thus, Cotton opposed referring to them as cluster materials.[16] At the time, this reasoning would be unchallenged considering that POMs were predominantly known for early transition metals in high oxidation states (*i.e.*, V^{5+}, Mo^{6+}, W^{6+}, Nb^{5+}, and Ta^{5+}) and in that form, they do not exhibit metal–metal bonding.[17,18]

Nowadays, many metal clusters can be seen as an extension to the chemistry of metal–metal bonded complexes (Fig. 1),[19,20] where the latter class is not only of fundamental relevance in inorganic chemistry,[21,22] but also has its practical

Department of Chemical Engineering and Biotechnology, University of Cambridge, Philippa Fawcett Drive Cambridge CB3 0AS, United Kingdom.
E-mail: aleksandar@kondinski.com; http://www.kondinski.com
† On leave from KU Leuven, Belgium.

Aleksandar Kondinski

*Aleksandar Kondinski is a Feodor Lynen Fellow at the University of Cambridge. He studied chemistry at Jacobs University Bremen, where he became fascinated with polyoxometalates (POMs) and their structure, formation and characterisation. As a doctoral candidate led by Prof. Thomas Heine, he worked further towards computational modelling and description of isomeric and metal–metal bonded POMs. After his promotion in 2016, he successfully completed two postdoctoral stages in applied POM chemistry at RWTH Aachen and KU Leuven as an awarded fellow. His research interests lie in the computer-aided development of electro-responsive functionalities in POMs and engineering of POM-based electronic systems (*i.e.*, "POMtronics").*

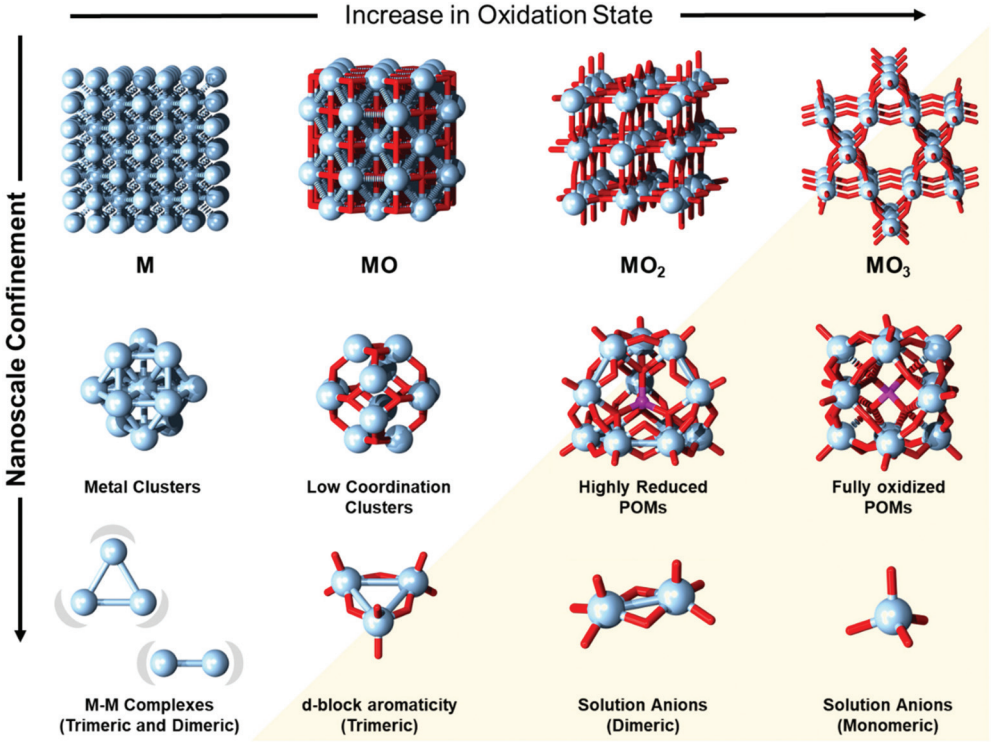

Fig. 1 Schematic representation of material evolution as a function of the oxidation state (top row, left to right) while confining the material class to nanoscale metal(oxo) clusters in terms of dimensionality and nuclearity (from top to bottom). Colour code: metals = light blue and O = red spheres.

role in biology,[23] catalysis,[23] and nanotechnology.[24,25] Modern POM chemistry also encompasses many other assemblies made of middle and late d-block elements (*e.g.*, Fe, Cr, Cu, Pd, Au, Pd, and Pt)[26,27] and f-block elements (*e.g.*, Np and U).[28] Over time, owing to the impressive stability of POMs,[29,30] their relevance in catalysis,[31,32] molecular magnetism,[33,34] and optics[35] has been significantly expanded.

At first sight, it appears that POMs and metal–metal bonds have very little chemistry in common. However, POMs boasting a high number of metal centres have repeatedly shown the ability to undergo multielectron redox processes that are rarely rivalled by other molecular compounds. This phenomenon, along with their facile preparation and production scalability, has been a cardinal point for their consideration in the development of "POMtronics", that is, POM-based electron storage and molecular electronics technologies.[36–40] In classical POMs, one-electron and two-electron reductions at each addenda centre lead to the formation of so-called highly reduced and super-reduced POMs, respectively.[41] These extreme reductions can trigger covalent dynamics and the formation of metal–metal bonds, which ultimately enriches POMs with cluster-like features. The global rush for a search of sustainable battery and supercapacitor materials has led to increased interest in the study of super-reduced POMs. In the literature, nowadays, one can find claims that tens to hundreds of electrons can be perfectly stored in a single POM while the POM supposedly retains its structural integrity.[42,43] When envisioning a similar process on the landscape of bulk metals and bulk metal oxides (Fig. 1), high reductions in metal oxides would be normally associated with the gradual lowering of the oxidation states, re-emergence of metal–metal bonding, increase in conductivity and eventually loss of the oxo ligands. Similarly, one may also question how such super-reductions affect the POM, the formation of metal–metal bonds and their role in the evolution of metal cluster-like behaviour. The limits of this transformation are also essential to ensure that the POM retains its structural integrity. Therefore, the entanglement of fundamental science and emerging technologies makes the discussion about the relationship between POMs, metal clusters and metal–metal bonds relevant again. Insights into this relationship can be important for devising the rational design of POMs with advanced covalently dynamic functionalities and for the use of POMs as unconventional all-inorganic ligands that simultaneously merge and expand the interrelated chemistries of these material groups.

The early studies of POMs decorated with metal–metal bonding moieties date back to the 1970s when Knoth[44,45] and Pope[46] made some pioneering synthetic discoveries. However, with the limited characterisation and computing resources available at the time, it must have been very challenging to continue advancing the research area. At the turn of the century, the list of POMs bearing metal–metal bonding functionalities increased, but this did not bring the metal–metal bonding features under the spotlight. Metal–metal bonded features in POMs were discovered along with other features which sometimes may have overshadowed the importance of metal–

metal bonding. For instance, the discovery of the ε-Keggin structure[47] has shown relevance in materials design, while different forms of polyoxothiometalates with metal–metal bonding have been of interest in proton conduction and catalysis.[48] Similarly, the metal–metal bonding[49,50] in Müller's $\{Mo_{132}\}$ Keplerate[51] has been overshadowed by the fascinating structural beauty of this POM.

With the rising popularity of density functional theory (DFT) and its applicability to POMs, many experimentally and conceptually derived POM models could be studied, providing ground for a deeper theoretical understanding.[52] This has been an important game-changer as before, theoretical insights were limited to bond valence sum calculations[53] and applications of Hückel theory.[54] The DFT studies made a paradigm shift in the discussion of the dominant concerns in metal oxo bonding in protonation to virtually all sorts of covalent bonds (*e.g.*, M–N,[55] M–S,[56] and M–O–C[57] bonds) and even ionic bonding between the POMs and the surrounding countercations.[58] These insights into what I would refer to as "static" bonding have provided the steppingstone to evaluate new forms of dynamic covalent bonding. An example of the latter is Cronin's redox responsive formation of Se–Se bonds in POMs, which have made a mark as "write-once-erase" memory storage materials.[40,59]

Many metal–metal bonded complexes exhibit impressive and reversible covalent dynamics. Considering the superior number of metals *versus* suitable non-metals (*e.g.*, Se), there are a plethora of opportunities for the development of covalently dynamic metal–metal bonded POMs that can be employed in the design of memristive POMtronics. Therefore, to develop deeper insights into the common chemistry between POMs and metal–metal bonds, the discussion in this article revolves around the nature of the reported metal–metal bonding in POMs. The first distinction is based on whether the metal–metal bonds are defined by the same or different types of metal centres (*i.e.*, homometallic *vs.* heterometallic). Many POMs that are plenary or "structurally saturated" exhibit only a single type of metal centre, and thus only homometallic bonding can evolve. In solution, some POM-building species may already exhibit metal–metal bonding, and thus the metal–metal bonding is transferred to the POM during the self-assembly process. An example of this would be the highly reduced ε-Keggin structure (Fig. 1). Homometallic bonding can also be electrochemically induced by reducing fully oxidised POMs. An example of the latter is the well-known α-Keggin structure (Fig. 1). The latter set of plenary and monometallic POMs with homometallic metal–metal bonds are discussed in section 2 of this article. When the POM structure has been defected by a formal loss of a $\{M_xO_y\}$ fragment, it can behave as an all-inorganic polydentate ligand and thus actively bind to other heterometals. These types of defected or lacunary POMs can incorporate pairs of heterometals that can establish homometallic (section 3) or heterometallic bonding in-between (section 4). Finally, a few examples of POMs that link to clusters or that incorporate heterometallic metal–metal bonded moieties within their cavities are introduced in section 5 of this article.

2. Homometallic metal–metal bonding between addenda centres

POMs are the most complex inorganic architectures that integrate from tens to hundreds of atoms.[60] Their complexity can be further complicated by their isomer problem[61] and their electronic structure.[52,62] Owing to this complexity, the direct description of the metal–metal bonds across many different systems may be very difficult. The latter challenge may require the use of some carefully implemented reductionism throughout our discussion. For a balanced description, the main part of this section focuses on underlining the relationship between the compatibility of the overall POM architecture and the constituting building blocks. To rationalise this approach a short overview of the electronic structure of POMs is provided first.

The electronic structure of POMs has been the focus of recent reviews.[52,63] To make an overview of the general properties of fully oxidised POMs, one, for instance, can consider the case of the Lindqvist-type hexamolybdate $[Mo_6O_{19}]^{2-}$ (Fig. 2a),[64] and compare it with the hexazirconate core $\{Zr_6O_8(HCO_2)_{12}\}$ that appears as a common building unit in reticular architectures.[65] Both structures have an overall O_h symmetry, where the six metal addenda centres occupy the vertices of a virtual octahedron. In $[Mo_6O_{19}]^{2-}$ each Mo^{6+} centre is terminated by a η-oxo ligand whilst the six Mo^{6+} centres are further interconnected by twelve μ_2-oxo ligands and one μ_6-oxo ligand that is encapsulated in the octahedron. For the hexazirconate we can consider the molecular model $[Zr_6O_8(HCO_2)_{12}]^{4-}$ that has been part of the theoretical discussion in the recent literature (Fig. 2a).[66] In $[Zr_6O_8(HCO_2)_{12}]^{4-}$

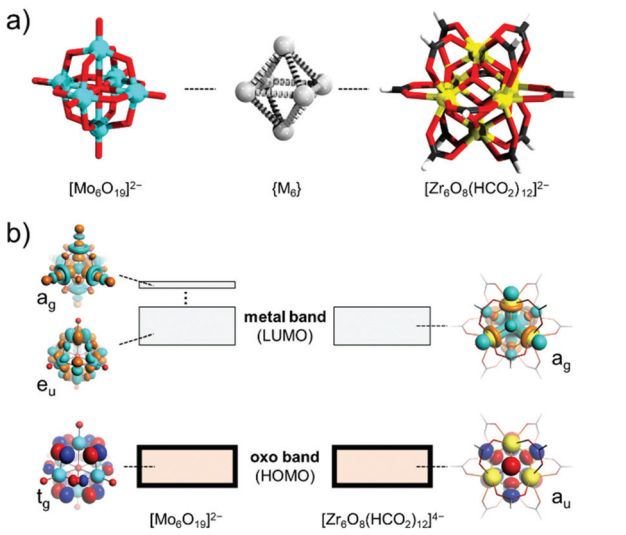

Fig. 2 (a) Ball and stick representation of the $[Mo_6O_{19}]^{2-}$ (left) and $[Zr_6O_8(HCO_2)_{12}]^{4-}$ model (right) showing the shearing $\{M_6\}$ octahedron in the middle. (b) Simple molecular diagram depicting the HOMO and LUMO(s) of the $[Mo_6O_{19}]^{2-}$ and the $[Zr_6O_8(HCO_2)_{12}]^{4-}$ model. The drawn orbitals correspond to previously reported theoretical studies.[64,66] Colour code: Mo = cyan, O = red, Zr = yellow, H = white, and C = black.

the six Zr^{4+} centres are interconnected by eight μ_3-oxo ligands and twelve formate-type μ_2-(HCOO) ligands. Both $[Zr_6O_8(HCO_2)_{12}]^{4-}$ and $[Mo_6O_{19}]^{2-}$ have a comparable distance between opposing centres (*ca.* 4.7 Å), however, one obvious difference is that the hexamolybdate hosts a single μ_6-oxo ligand and the hexazirconate does not. The highest occupied molecular orbitals (HOMOs) in these systems are exclusively O-centred featuring p-type orbitals compared to the so called "oxo band" in bulk metal oxides (Fig. 2b).[52,63] On the other hand, the lowest unoccupied molecular orbital (LUMO) typically (de)localises predominantly over the metal centres, resembling the "metal band" in the bulk.[52,63] In the case of $[Zr_6O_8(HCO_2)_{12}]^{4-}$ one can notice that there is significant delocalisation over the Zr-centred d_{z^2} orbitals and on the O-centred p-type orbitals leading to the overall a_g molecular orbital. The a_g orbital exhibits constructive interference of Zr-centred d_{z^2} orbitals in the cavity of the model and antibonding features along the Zr–O bonds. The equivalent a_g orbital in $[Mo_6O_{19}]^{2-}$ does not serve as a LUMO, and thus lies higher in energy. The reason is that the central μ_6-oxo ligand also provides an s-atom like orbital which serves as an antibonding node between the six Mo-centred d_{z^2} orbitals. The actual LUMO in $[Mo_6O_{19}]^{2-}$ delocalises over the doubly degenerate e_u-type orbitals featuring Mo-centred d_{xy}-type orbitals and O-centred p-type orbitals (Fig. 2b). Along the Mo–O axis, the e_u-type LUMO is displaying an antibonding feature which implies that significant reductions can lead to ligand destabilisations. In other words, the presence of the central oxo ligand may stabilise the formation of $[Mo_6O_{19}]^{2-}$ and at the same time hamper the facile formation of metal bonding between the six Mo centres due to their highly reduced states. From the examples provided at the end of this chapter, the bonding situation may be changed when symmetry breaking occurs or when the central oxo ligand is formally removed.

The two examples show that in POMs and in other fully oxidised metal oxo clusters that are based on early d-block elements, the population of the "metal band" (*i.e.*, the LUMOs) introduces some anti-bonding features between the metal and the oxo ligands but depending on the archetype, it can also lead to bonding features between the addenda centres. The "metal band" population makes the charge of the POM higher, which also attracts stronger binding of countercations that bring some stabilisation.[67] However, the stretch of this balancing across different structures, oxidation states and POM archetypes has not been systematically studied, which limits our discussion here. The electron population of the "metal band" is also followed by stepwise evolution of bonding, which in some scenarios has the propensity to localise, triggering symmetry breaks and increases in strain. The latter aspects provide a possibility to carry a further discussion with consideration of a metal–metal bonded building block and answering how that building block integrates into the framework of the POM archetype.

In a complete and isolated POM structure, one can identify different fragments which once virtually parsed can be used to describe a set of elusive building blocks differing in shape and connectivity.[67] These fragments often derive from solution species[68] that are mononuclear, dinuclear, and tri-nuclear and that have been integrated following condensation processes.[29] Among late transition metal POMs, one may commonly observe planar $\{MO_4\}$ elusive building blocks.[69] Among the early transition metal based POMs (*e.g.*, V^V, Mo^{VI}, and W^{VI}), square pyramidal $\{MO_5\}$ or quasi-octahedral $\{MO_6\}$ elusive building blocks are more prevalent. The latter is because of the good stabilisation of the terminal oxo ligands by such centres.[70] To connect two $\{MO_4\}$ or $\{MO_5\}$ building blocks through a metal–metal bond, one can envision two scenarios. First, the two metal centres may be connected directly along their four-fold axes, *i.e.* $\{O_5M–MO_5\}$-type assemblies (Fig. 3a). This connectivity is manifested among some late transition metal complexes that build "paddlewheel"-like species (*e.g.*, Pt^{III}). Second, the metal centres may be connected through a metal–metal bond that propagates along with the two bridging μ_2-oxo ligands. The latter feature is common among dinuclear $Mo^{IV/V}$ and $W^{IV/V}$ oxo complexes in water, where the electrons from the local d_{xy}-orbitals constructively interact and overlap (Fig. 3b).[71] The aquatic complexes of dimeric metal–metal connected $[Mo_2O_4]^{2+}$ and $[W_2O_4]^{2+}$ are very stable.[72] Connectivity between three centres leading to cyclic $\{M_3O_9\}$ where M = Mo and W is also possible, and it is enabled through the constructive overlap of the d_{z^2} atom-like orbitals of the adjacent metal centres (Fig. 3c).[73] In solution, Mo^{IV} and W^{IV} form stable trinuclear $[Mo_3O_4]^{4+}$, and $[W_3O_4]^{4+}$ aquatic cores,[74,75] that can be described as assemblies of three $\{MoO_6\}$ octahedra sharing a common vertex and an edge for each pair. The metal–metal bond connectivity occurs *via* three-centre two-electron bonds (Fig. 3d).[76] In these aquatic cores, the aqua ligands can be easily substituted with other ligands, forming a variety of derivatives such as $[Mo_3O_4(C_2O_4)_3(H_2O)_3]^{2-}$,[74,77] which can be used as precursors in chemical synthesis.

From the outline, we identify three general metalate building blocks that can participate in the construction of POMs. As late transition metal-based POMs are less prevalent, the utility of $\{O_5M–MO_5\}$ type building units is also rare. Such units are not very flexible and require to be interlocked with other ligands. In this regard, Pt^{III} cations with oxo and sulphate ligands can build the Wickleder structure $[Pt_{12}O_8(SO_4)_{12}]^{4-}$ which exhibits an ideal and rare pyritohedral symmetry (Fig. 3e).[78,79] The $[Pt_{12}O_8(SO_4)_{12}]^{4-}$ polyanion can be described as a condensation of six $\{Pt_2O_4\}$ handle-like moieties which form a cuboidal $\{Pt_{12}O_8\}$ subunit that has been capped and interlocked by 12 μ_3-(SO_4) tetrahedra. The $\{Pt_{12}O_8\}$ subunit is virtually identical to the building motif in the bulk waserite $Na_xPt_3O_4$ structure, also known as Adams' catalyst.[80] In comparison to the "ideal" arrangement in the waserite structure, the metal-oxo core of $[Pt_{12}O_8(SO_4)_{12}]^{4-}$ exhibits contractions and distortions (*i.e.*, strain). These distortions derive from the unequal ligand environment around the Pt^{III} centres and the presence of Pt–Pt bonds, which are shorter than the Pt⋯Pt contacts in the waserite structure by some 0.3 Å. The geometric strain plays a major role in the overall bonding energies in POMs and their relative stabilities.[81] The electrochemical pro-

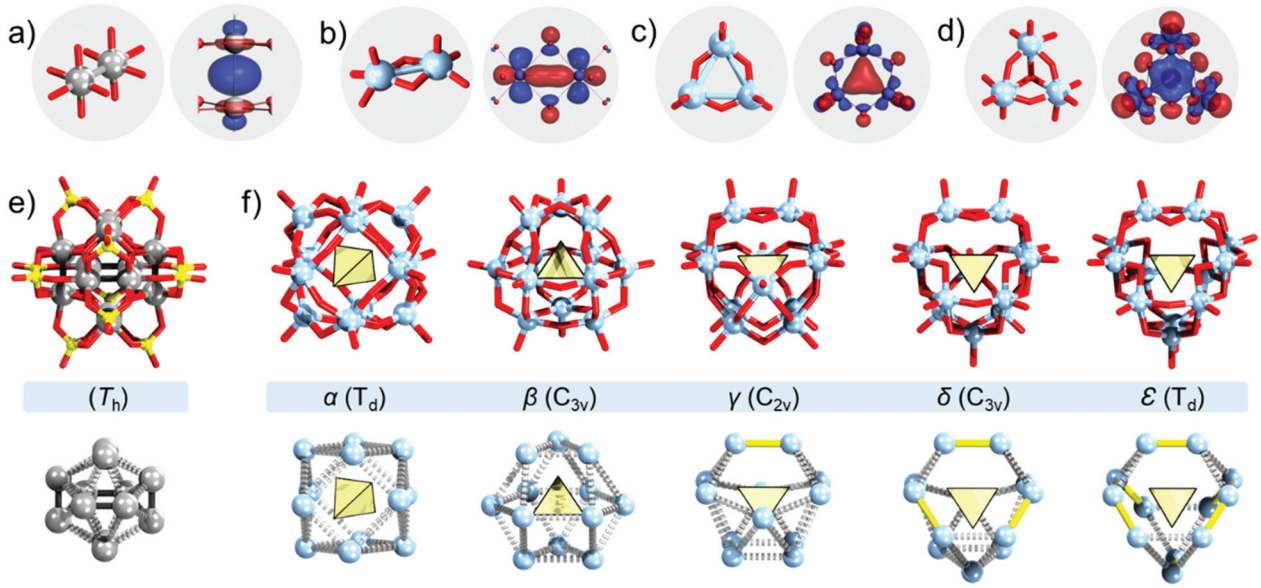

Fig. 3 Ball and stick representation along with examples of bonding orbitals (recalculated and redrawn from ref. 93 and 106) within particular metal oxo species: (a) $\{Pt_2(OH)_8(aq)_2\}$ and interaction of d_{z^2}; (b) $\{Mo_2O_8\}$ and interaction of d_{xy}; (c) $\{Mo_3O_9\}$ and (d) $\{Mo_3O_{13}\}$ with the interaction of their d_{z^2}. (e) $[Pt_{12}O_8(SO_4)_{12}]^{4-}$ and $\{Pt_{12}\}$ core; (f) Baker–Figgis isomers of the Keggin $[(XO_4)M_{12}O_{36}]^{n-}$ anions and the $\{M_{12}\}$ cores. Colour code: Pt = grey, Mo/M = light blue, O = red, and S = yellow.

perties of the $[Pt_{12}O_8(SO_4)_{12}]^{4-}$ system have not been explored yet; however, a potential reduction of this POM may destabilise the bonding along the {O–Pt–Pt–O moieties} potentially leading to the molecular actuator functionality that is relevant in molecular electronics.

Although there is an absence of configomers to Wickleder's dodecaplatinate that can enable cross-structural comparison, the geometric features and their effect on relative stability are more prevalent in the classical POMs. The well-known α-Keggin $[(XO_4)M_{12}O_{40}]^{n-}$ can be viewed as an inorganic host–guest system, where a central $\{XO_4\}$ heterogroup is encapsulated by a shell of twelve $\{MO_5\}$ square pyramids, *i.e.*, an α-$\{M_{12}O_{36}\}$ shell.[26] In the α-$\{M_{12}O_{36}\}$, the twelve addenda centres constitute the corners of a virtual and idealised cuboctahedron. Five different configurational isomers, classically known as Baker–Figgis isomers and denoted as α-/β-/γ-/δ-/ε-Keggin, can be derived by formal and stepwise rotation of triad $\{M_3O_{13}\}$ units by 60° (Fig. 3f).[82] In the α- and β-Keggin topology, all $\{MO_5\}$ square pyramids are only corner-sharing. In γ-, δ- and ε-Keggin, $\{MO_5\}$ square pyramids start to share edges, forming one, three, and six $\{M_2O_8\}$ building units, respectively. Experimentally fully oxidised metal species adopt α- and occasionally β-Keggin topology.[26] From the calculated total energy of $[(XO_4)M_{12}O_{40}]^{n-}$ with M = Mo^{VI} and W^{VI}, the stability trend follows the order α > β > γ > δ > ε.[83] The order is logical, considering that the addenda centres are highly positively charged. The M···M separation from the corner-sharing arrangement (*ca.* 3.1 Å) is significantly reduced in the edge-sharing arrangement (*ca.* 2.8 Å), which causes Coulomb repulsions. However, when instead of fully oxidised (*e.g.*, Mo^{VI}), reduced and Mo–Mo bonded species are employed such as $[Mo_2^V(\mu\text{-}S)_2O_2]$ in α-/β-/γ-/δ-/ε-$[(Mo^{VI}O_4)Mo_{12}^VO_{12}S_{12}(OH)_{12}]^{2-}$, the stability order is reversed.[84] The change in the stability order can be explained based on the dissociation of the metal–metal bonds, which aid the delocalisation of the excess electron charges in the POM cluster.[84] In practice, fully oxidised polytungstates form incomplete, unsaturated (*i.e.*, lacunary) γ-Keggin polyanions such as $[SiW_{10}O_{36}]^{8-}$. Although the latter POM does not incorporate an $[M_2^{VI}O_4]^{4+}$ fragment, it can be functionalised with a metal–metal bonded $[M_2^VS_2O_2]^{2+}$ unit forming solution stable γ-$[SiW_{10}M_2S_2O_{38}]^{6-}$ POMs (M = Mo^V, W^V).[85] The γ-$[SiW_{10}M_2S_2O_{38}]^{6-}$ systems can then be reversibly oxidised and reduced in DMF, leading to observable colour changes.[86] Considering that their redox chemistry is linked to the dissociation and reformation of the Mo–Mo bonding moiety, Cadot and coworkers recently indicated this system as relevant in electrocatalysis and electrosensing.[86]

At this point, one may draw two conclusions: (i) the changes in the overall topology can induce changes in the local parameters that affect individual building blocks; (ii) the electronic changes in a minimal building block can induce metal–metal bonding and alter the local geometric parameters, which then subsequently impact the stability of the overall POM structure. The second conclusion is not universal and does not apply to all POMs for all types of reductions. For instance, the high reduction of the fully oxidised vanadium Kegginoid $\{V_{18}^VO_{42}\}$ to $\{V_{18}^{IV}O_{42}\}$ is not associated with significant geometric changes as there is an absence of metal–metal bond formation that otherwise would have contracted the cluster.[87] In the case of molybdenum, the oxidation state influences the solution chemistry, and consequently, the library of intermediate building blocks participating in the POM for-

mation. When analysing the structure of ε-Keggin, one can simply describe it as a tetrahedron constructed of six edge-sharing $\{M_2O_{10}\}$ units hosting a central $\{XO_4\}$ heterogroup. As five and four valent molybdenum are typically dimeric, edge-sharing species in solution, one can postulate that ε-Keggin would normally be associated with highly reduced POMs. Indeed, in 2002 Mialane and coworkers reported the first ε-Keggin of molybdenum as a tetra-lanthanide(III) adduct, that is ε-$[PMo_{12}O_{36}(OH)_4\{La(H_2O)_4\}_4]^{5+}$.[47] The isolation as an adduct may have appeared initially as a disadvantage; however, it has been shown to be very useful in the design of tetrahedral nodes where zinc(II) adducts of the ε-Keggin connect with branching organic ligands, leading to the construction of POM based organic frameworks (Fig. 4a),[88] with potential applications in hydrogen evolution,[88] nitrite reduction,[89] and energy storage.[90] The ability of the ε-Keggin to construct POM based organic frameworks and to be involved in a wide range of electrocatalytic applications may have to do with its electronic and atomistic structure. On the basis of ^{95}Mo NMR and DFT calculations, Nishimura and coworkers have concluded that the electron density in this POM remains delocalised.[91] This implies that redox processes may populate/depopulate the Mo–Mo bonding in ε-Keggin, however, without inducing symmetry breaking, which is needed when considering its role as a node in a highly symmetrical framework structure. On the other hand, multielectron reductions in the α-Keggin lead to the formation of metal bonding within localised $\{Mo_3\}$ triads, which subsequently induces contractions and symmetry breaking (*vide infra*). This delocalisation *vs.* localisation property with the generation of Mo–Mo bonding is something that obviously differentiates ε-Keggin and α-Keggin and the domains of their applicability.

Similarly, as in ε-Keggin, the dimeric $\{Mo^{V}_2O_8\}$ units constitute an important building block of Müller's $[Mo^{VI}_{72}Mo^{V}_{60}O_{372}]^{72-}$ $\{Mo_{132}\}$ Keplerate architecture (Fig. 4b).[51] In the latter structure, twelve pentagonal $\{Mo^{VI}_6O_{11}\}$ units occupy corners of a virtual icosahedron, while thirty linear $\{Mo^{V}_2O_8\}$ units link them. The combination of metal-oxo and metal–metal bonding in $\{Mo^{V}_2O_8\}$ units has been associated with strong structural rigidity enabling the formation of the overall large $\{Mo_{132}\}$ architecture.[92] The highest occupied molecular orbitals in the latter polyanion are elegantly delocalised between the paired Mo^{V} centres of each linking unit.[93] Müller's $\{Mo_{132}\}$ and its derivatives have been overwhelmingly covered in many excellent reviews ranging from molecular magnetism[94] and homogeneous catalysis[95] to supramolecular chemistry.[96] The linking nature of the $\{Mo_2O_8\}$ moieties is also noticed in Kabanos' $[(Mo^{V}_2O_4)_3(\mu_2\text{-}O)_3(\mu_2\text{-}SO_3)_3(\mu_6\text{-}SO_3)]^{8-}$ polyanion which in the solid-state dimerises with the help of a single sodium cation, forming $[Na\{(Mo^{V}_2O_4)_3(\mu_2\text{-}O)_3(\mu_2\text{-}SO_3)_3(\mu_6\text{-}SO_3)\}_2]^{15-}$ (Fig. 4c).[97] The monomeric hexamolybdate unit consists of three dimolybdate units in which the distance of the Mo^{V} pairs is only 2.56 Å. The dimolybdate moieties are interconnected *via* edge-sharing, three outer and one central

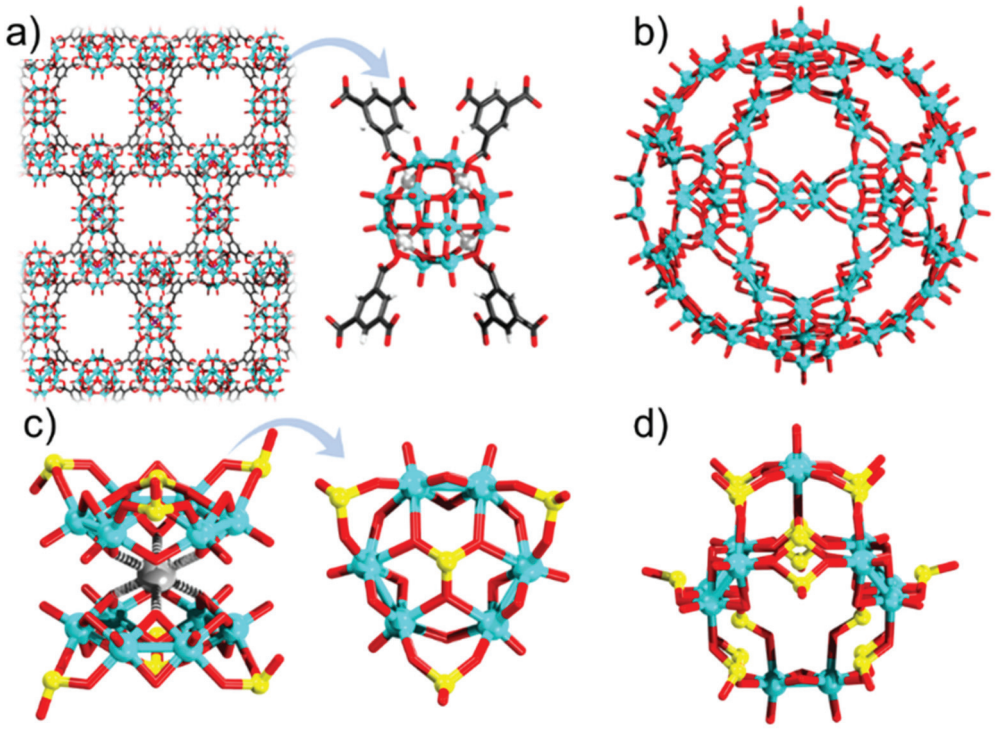

Fig. 4 Ball and stick representation of (a) framework with 1,3,5 benzene tricarboxylate; (b) $[Mo^{VI}_{72}Mo^{V}_{60}O_{372}]^{72-}$; (c) $[Na\{(Mo^{V}_2O_4)_3(\mu_2\text{-}O)_3(\mu_2\text{-}SO_3)_3(\mu_6\text{-}SO_3)\}_2]^{15-}$ and its monomeric unit; (d) $[(Mo^{V}_2O_4)_6(\mu_2\text{-}SO_3)_{12}(\mu_6\text{-}SO_3)_4]^{20-}$ structures. Colour code: Mo = cyan, O = red, Zn = light grey, H = white, C = black, S = yellow, and Na = dark grey.

sulphite unit. The dimeric structure is synthesised in acidic media by reducing $Na_2Mo^{VI}O_4$ with hydrazine and condensation with $(NH_4)SO_3$. The sodium bridge dimer is a useful reducing agent for $[Au^{III}Cl_3OH]^-$ and for the controlled formation of gold nanoparticles.[98] Based on careful molecular modelling and DFT calculations, Lang and coworkers have revealed that two electrons coming from each Mo–Mo group can reduce the Au^{III} precursor to Au^{I}, subsequently promoting the nucleation of the Au-nanoparticles.[97] This implies that in the absence of the Mo–Mo bonding functionality in this POM, its application in the formation of gold nanoparticles would not have been possible.[98] Careful adjustments of the starting conditions lead to the larger cage-like polyanion $[(Mo_2^{V}O_4)_6(\mu_2\text{-}SO_3)_{12}(\mu_6\text{-}SO_3)_4]^{20-}$ (Fig. 4d), where the $\{Mo_2^{V}O_8\}$ units are interconnected *via* twelve μ_2-SO_3^{2-} and four μ_6-SO_3^{2-} ligands. In these assemblies, the Mo–Mo bond lengths are *ca.* 2.60 Å.[99]

The triads in fully oxidised α-Keggin are structurally different from those in the reduced trimeric molybdate species. The Mo···Mo distances in a fully oxidised Keggin triad $\{Mo_3O_{13}\}$ are about 3.3 Å. In contrast, the Mo–Mo bonds in the free unstrained triad $[Mo_3O_4(C_2O_4)_3(H_2O)_3]^{2-}$ are *ca.* 2.5 Å. At the same time, the terminal oxo ligands in a Keggin triad are 1.6 Å away while the aqua ligands in $[Mo_3O_4(C_2O_4)_3(H_2O)_3]^{2-}$ lie some 2.1 Å away. In this regard, the full reduction of a triad in a classical POM will be expected to introduce structural changes; that is, the POM becomes more strained and increases its overall negative charge and reactivity. The interest in overloading the POM with electrons is almost a half-century old. Originally, Launay first probed the electrosynthesis and the high reduction of POMs in 1976.[100] It was discovered that when metatungstate $[H_2O_4W_{12}O_{36}]^{6-}$ is being reduced, blue species form.[100] In these species, the electrons are delocalised over all W-centres. However, with a reduction of six electrons per Keggin, there is an emergence of qualitative changes. The electrons become localised within a single triad, turning the colour of the species to brown. It was noted that other very stable forms with 12, 18, and 24 electron reductions form, but they also precipitate.[101] The formation of the six electron reduced species for $[X^{n+}O_4W_{12}O_{36}]^{[8-n]-}$ species (X = H_2^{2+}, B^{3+}, Si^{4+}) has been confirmed based on crystallography and ^{183}W NMR.[102–104] Similarly, in these POMs, the reduction causes the W···W distance within a particular triad to shrink from 3.3 Å to 2.5 Å. Following these reports, Pope showcased that after electrochemical generation of $[X^{n+}O_4W_{12}O_{36}]^{[8-n]-}$ species (X = H_2^{2+} and B^{3+}), the formed species can be reacted with sodium tungstate and thus can form $[(XO_4)W_3^{IV}W_{17}^{VI}O_{62}H_x]^{y-}$ (X = H_2^{2+}, B^{3+}).[105] The added tungstate units replace aqua and bridging oxo/ligands from the highly reduced triad, leading to the addition of a new $\{W_8^{VI}O_{30}\}$ unit (see Fig. 5a). This implies that the generation of the tungsten–tungsten bonding has subsequently altered the chemical reactivity of the latter POM set. The $[(XO_4)W_3^{IV}W_{17}^{VI}O_{62}H_x]^{y-}$ POMs have been fully characterised on the basis of elemental analysis, ^{183}W NMR, and X-ray crystal structure analysis.

With the increased demand for the development of batteries and supercapacitors, the research in multielectron storing POMs has been of growing interest.[57,90,106] In 2014, the Awaga group reported that α-$[PMo_{12}O_{40}]^{3-}$ can be used as an active cathode material with a lithium metal anode. The α-Keggin has been reported to have a capacity of 270 A h kg^{-1} in the voltage range 4.0 to 1.5 V. Based on X-ray absorption near-edge structure analysis, it has been showcased that all Mo^{VI} is reduced to Mo^{IV} during the discharge process. The X-ray absorption fine structure spectrum is qualitatively similar to that of the DFT simulated one for α-$[PMo_{12}O_{40}]^{27-}$.[107] Based on the DFT calculations, the T_d-symmetrized α-$[PMo_{12}O_{40}]^{27-}$ shows the formation of $\{Mo_3\}$ triangles within its triad $\{Mo_3O_{13}\}$ units. In a subsequent study, the Irle group provided a ground state DFT description of α-$[PMo_{12}O_{40}]^{27-}$ (T_d) and molecular dynamics description of the POM in the presence of Li^+ cations.[106] The results showed that once the symmetry constraints are removed, the α-$[PMo_{12}O_{40}]^{27-}$ eventually dissociates. However, before the dissociation, that is 1.113 ps from the beginning of the MD process, the highly charged POM starts to undergo significant structural rearrangements. The authors noted that instead of the four $\{Mo_3\}$ triangles, "two triangular Mo sites, two single Mo–Mo bonds, and even one Mo=Mo double bond" are formed. The structural rearrangements are energetically favourable by some 2.95 eV (67.9 kcal mol^{-1}). This has been attributed to the changes in the Mo bonding or the arrangement of the Li cations, although after careful inspection, it may be more likely due to an uncontrolled dissociation of the first Mo–O bond, which balances the high strains within the cluster (see Fig. 5b). The authors indirectly refer to the dissociation as super-reduced α-Keggin has a "semiporous molecular" nature. These aspects clearly show some shortcomings on the side of the super-reduced α-Keggin and on the appropriateness of the fully symmetrised model. However, the study of POMs in super-reduced states is challenging and represents an uncharted research area, and thus precautions are needed. The absence of direct criticism of this work may have motivated the desire to outperform it. Recently it has been reported that the Keplerate $[Mo_{72}^{VI}V_{30}^{VI/V}O_{225}]^{25-}$ can be reduced with up to 472 electrons to form $[Mo_{72}^{I}V_{30}^{I}O_{225}]^{497-}$.[43] Both $Mo^{I/II}$ and $V^{I/II}$ are associated with the formation of strong metal–metal bonds.[108] As seen from the work of Irle and coworkers, once the reduction reaches Mo^{IV},[106] there is a change in the coordination and formation of metal–metal bonds and probably strain triggered dissociation of bridging oxo ligands which are difficult to control by lithium countercations. In this regard, the further strengthening of the metal–metal bonding character correlates with the destabilisation of the metal-oxo character, which makes such proposals unsupported and doubtful. However, purposely because of this, synthetic approaches using precursors that already contain metal–metal bonds, performing the synthesis in the presence of less negative bridging ligands (*e.g.*, alkoxy), and theoretical insights are critical to the understanding of how charge influences covalent dynamics in POMs.

The group of Xu pioneered a strategy in using the $[M_3O_4]^{4+}$ cluster for the preparation of Mo–Mo bonded polyoxomoly-

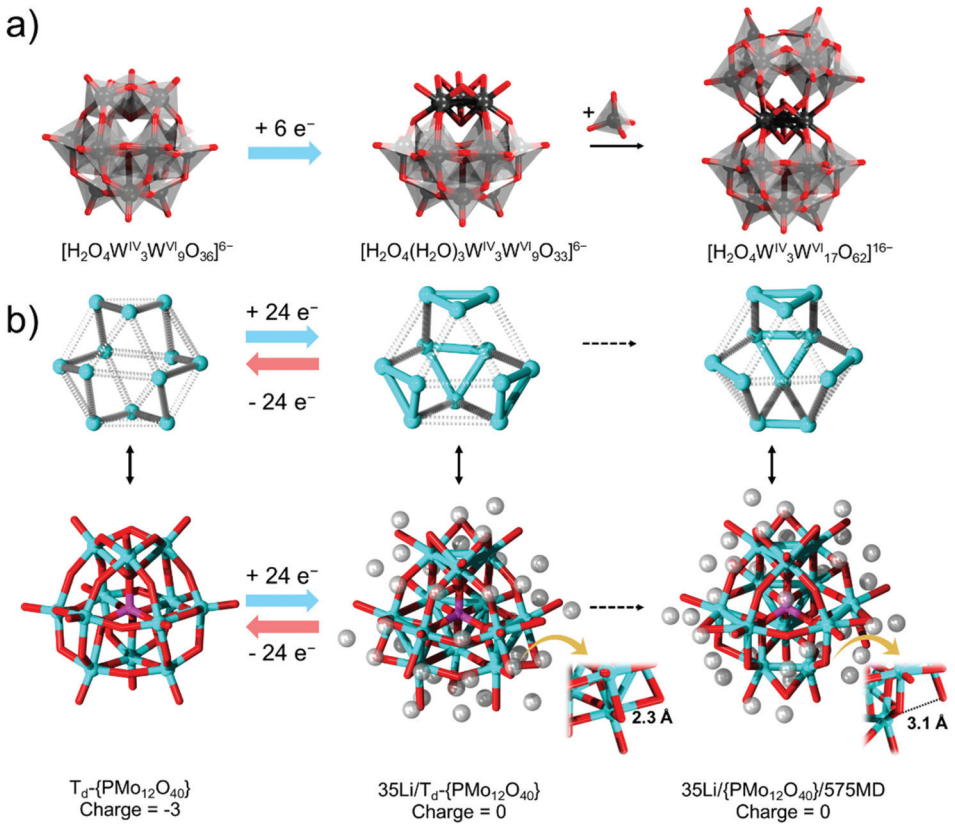

Fig. 5 Schematic representation of (a) subsequent six electron reduction of metatungstate and reaction of the formed $[H_2O_4(H_2O)_3W^{IV}_3W^{VI}_9O_{33}]^{6-}$ with sodium tungstate; (b) parallel representation of the addenda metal topologies (top row) and the overall models (bottom row) derived from DFT (BP86-D/SV(P) level) and MD calculations starting with a fully oxidised $[PMo_{12}O_{40}]^{3-}$ unit (left) moving to the optimised $[PMo_{12}O_{40}]^{27-}$ unit that was immersed in an environment with 35 Li centres (middle) and following up with MD calculations after 575 steps (right). Zoomed features for two models are shown, and all geometries were obtained from the supporting information of ref. 106. Colour code: $\{W^{VI}O_6\}$ = grey octahedral, W^{IV} = black, Mo = cyan, O = red, H = white, and Li = transparent grey spheres.

bates. The first structure reported by this group is $[Mo^{IV}_6Mo^{VI}_7O_{32}(OH)_4(py)_6]^{2-}$ (py = pyridine), which featured the β-Keggin isomer with two triangular $\{Mo_3\}$ units that are additionally capped with a cationic $\{MoO_2\}$ unit.[109] The first polyanion was produced with the help of the $[Mo_3O_4(Hnta)_3]^{2-}$ (where Hnta = nitrilotriacetic acid) precursor,[110] although in the follow-up studies the $[Mo_3O_2(O_2CCH_3)_6(H_2O)_3]^{2+}$ precursor was employed.[74] Some of the follow-up studies involve reports on $[Sb^{III}_3Mo^{IV}_3Mo^{VI}_{15}O_{55}(OH)_2(py)_3]^{-}$,[111] $[Mo@Mo^{IV}_6Mo^{V}_6Mo^{VI}_9O_{54}(OH)_4(py)_6]^{4-}$,[112] and $[Na@Mo^{IV}_{12}Mo^{V}_4Mo^{VI}_3O_{43}(OH)(py)_{12}]$ (all in Fig. 6).[113] These polyanions have peculiarities in terms of structure, and they have been outlined in great detail in the primary literature. Here an interesting aspect is the arrangement of the Mo centres in these systems. By close analysis, the ideal topologies of a fully oxidised species are likely to obtain high symmetries. By juxtaposing them to the experimentally resolved species, one can clearly see the contractions caused by the $\{Mo_3O_4\}$ triads and the Mo–Mo bonds. Even when starting from a reduced precursor with triangular $\{Mo_3O_4\}$ moieties, single Mo–Mo bonds are generated, and there are many sites that show an absence of Mo–Mo bonds probably due to reoxidation of the $Mo^{IV/V}$ centres. In larger structures, the triad and the Mo–Mo bond distribution appear to occur in a symmetrised fashion; however, more systematic follow-up DFT calculations would be beneficial. From these results, the rearrangements of the metal–metal bonds in the super-reduced Keggin[106] appear plausible (*vide supra*). With the addition of different hetero-groups (*e.g.*, PO_4^{3-} and GeO_4^{3-}) the group of Xu also discovered the formation of $[Mo^{IV}_3Mo^{VI}_{10}Zn(PO_4)_4(OH)_2O_{31}py_3]^{2-}$,[113] and $[Mo^{IV}_6Mo^{VI}_{10}Ge_3O_{48}py_6]$,[112] which can be described as lacunary POMs incorporating triangular moieties.

In 2020 Xu reported an advanced $\{Mo_{34}\}$ POM,[114] and considering the guidelines of highly symmetric POMs,[94] it can be regarded as a Keplerate topology. The $\{Mo_{34}\}$ follows the discovery of Brechin's $\{Fe_{34}\}$, which has a comparable topology and building up principle.[115] The $\{Mo_{34}\}$ can be described as an assembly of three main components (Fig. 7a). The inner core of the POM is a tetrahedra $\{M_4O_{10}\}$ cluster (M = Al, V, Mo). This cluster is encapsulated by a metal-oxo $\{Mo_{18}O_{102}\}$ cage constructed by six linear $\{Mo_3O_{11}\}$ triads. The cage faces are capped by four $[Mo_3O_4]^{4+}$ units, indicating that the $[Mo_3O_4]^{4+}$ units may also induce an outer templating effect. Each $[Mo_3O_4]^{4+}$ unit further binds to three pyridine molecules.

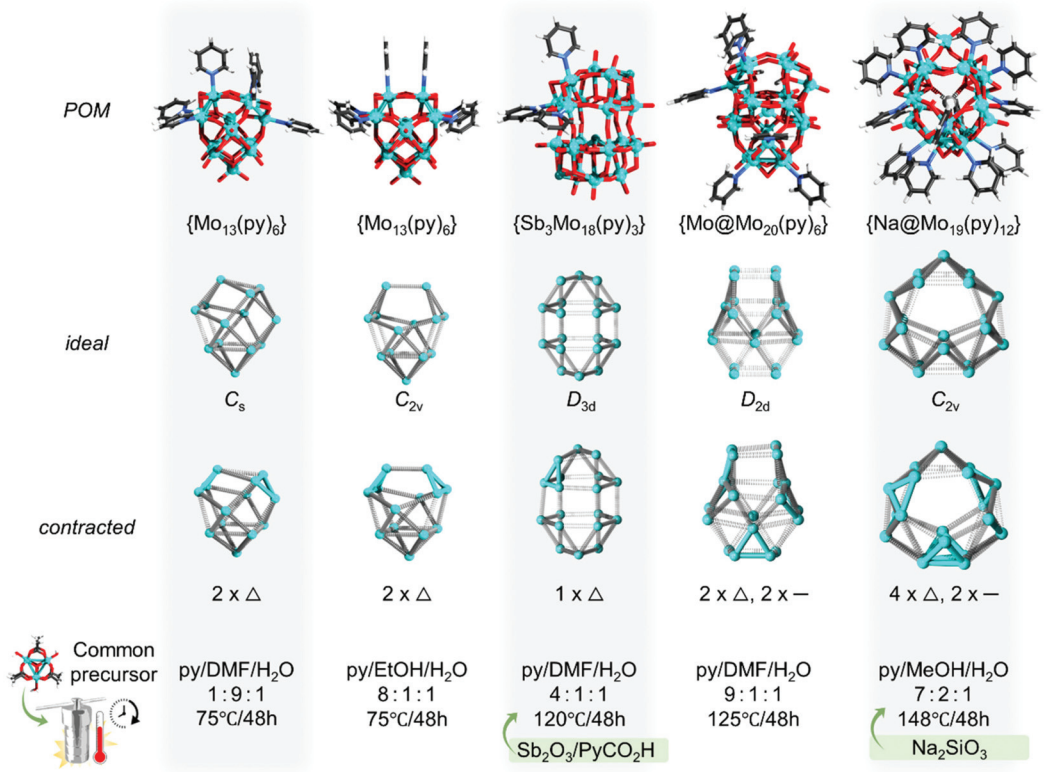

Fig. 6 Ball and stick representation of $[Mo^{IV}_{6}Mo^{VI}_{7}O_{32}(OH)_4(C_5H_5N)_6]^{2-}$ β and γ isomers, $[Sb^{III}_{3}Mo^{IV}_{3}Mo^{VI}_{15}O_{55}(OH)_2(py)_3]^{-}$, $[Mo@Mo^{IV}_{6}Mo^{V}_{6}Mo^{VI}_{9}O_{54}(OH)_4(py)_6]^{4-}$, and $[Na@Mo^{IV}_{12}Mo^{V}_{4}Mo^{VI}_{3}O_{43}(OH)(py)_{12}]$ all aligned in the top row, with their all-addenda topologies in idealised form (second row), contracted form as experimentally determined (third row) and the general conditions of their synthesis (fourth row). Colour code: Mo = cyan, O = red, N = blue, C = black and H = white spheres.

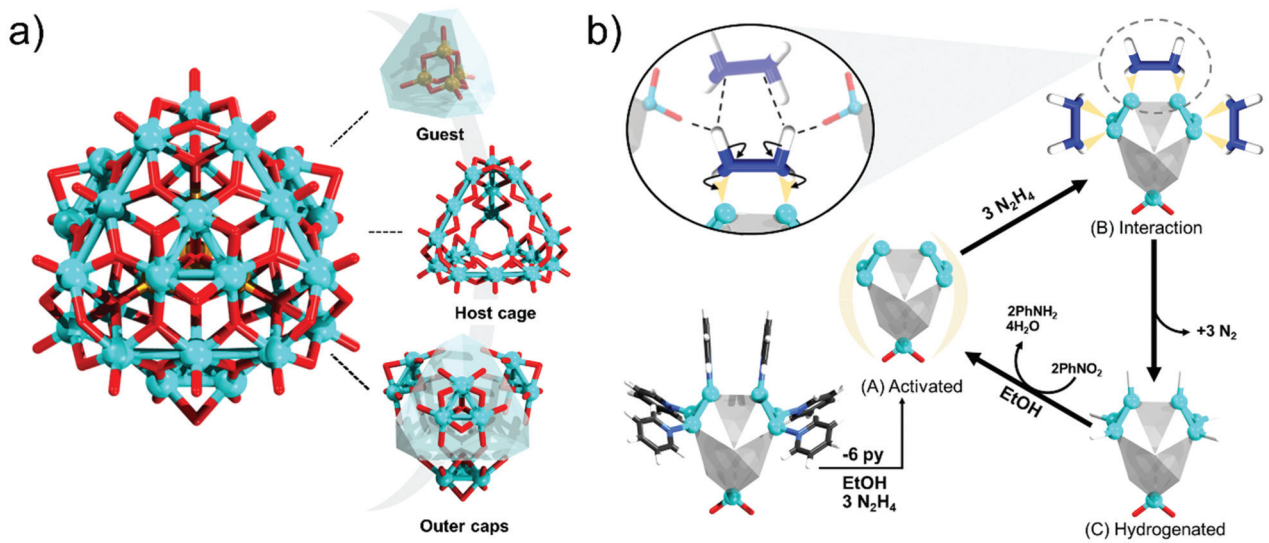

Fig. 7 Ball and stick representation of (a) $\{Mo_{34}\}$ with its subcomponents; (b) proposed catalytic cycle for $[Mo^{IV}_{6}Mo^{VI}_{7}O_{32}(OH)_4(C_5H_5N)_6]^{2-}$ (shown in simplified form) involved in the reduction of nitrobenzene. Colour code: Mo = cyan, O = red, N = blue, C = black and H = white spheres.

The particular polyanion appears structurally impressive and likely can maintain stability among multiple redox states, making it promising for the design of memristive devices. The current drawback of this POM is that it also co-forms in the presence of kegginoidal ions, and thus further synthetic optimisations may be desirable.

The original motivation of Xu's work was the development of hydrogenation catalysts based on frustrated Lewis pair systems that involve highly reduced POMs with partial cluster-like and partial metal-oxo features.[112,113,116] In this line, the γ-isomer of $[Mo_6^{IV}Mo_7^{VI}O_{32}(OH)_4(C_5H_5N)_6]^{2-}$ is a representative system that has shown an exceptional heterogeneous catalytic conversion of nitrobenzene to aniline with a yield of over 99% under mild conditions (Fig. 7b).[116] The Xu group has elaborated that in the presence of protic solvents and hydrazine, the pyridine ligands of the Mo^{IV} site are replaced, and the POM is then activated. Following this, it is proposed that a hydrazine molecule approaches a pair of Mo^{IV} sites that act as Lewis acids. At the same time, a Mo–O unit from a neighbouring POM acts as a Lewis donor and enables a second hydrazine molecule to approach. This arrangement provides spatial confinement for forming a six-centred $N_2H_2N_2$ ring, which results in heterolytic dissociation of the H atoms, hydrogenation of the POM, and formation of a leaving N_2 molecule. The hydrated POM then participates in the hydrogenation of $PhNO_2$ to $PhNH_2$ followed by the formation of H_2O molecules, and the overall cycle is then repeated. Although Xu did not present further theoretical insights into this work, the presence of metal–metal bonding makes the bonding of the terminal pyridine units more labile, thus providing an opportunity for exchange with hydrogen atoms which is not the case for fully oxidised POMs. From recent studies in a comparable system, the molybdenum triad would also be expected to undergo reversible covalent dynamics, enabling the continuation of the catalytic cycle.[117]

Formal replacement of the oxo ligands with less charged polyalkoxometalate ligands can allow higher reductions while maintaining a relatively low overall negative charge of the polyalkoxometalates. Such chemistry currently is most prominent and developed among polyalkoxovanadates; however, there is an absence of reports with metal–metal bonds.[118] To the best of our knowledge, currently, there are two polyalkoxometalates that exhibit metal–metal bonds and formally derive from the Lindqvist structure $[M_6O_{19}]^{n-}$ (see Fig. 8). The classical Lindqvist structure is a hexametalate, where the six addenda centres occupy the vertices of a virtual octahedron. The metal centres hold terminal oxo ligands, and they are interconnected with twelve bridging μ_2-O ligands. In the cavity of the POM, there is a central μ_6-O ligand. In polyalkoxomolybdates, the formal replacement of the terminal and bridging oxo units with terminal and bridging ethoxo ligands, respectively, and formal reduction virtually lead to the alkoxoPOM $[Mo_6O(OC_2H_5)_{18}]$.[119] The latter POM exhibits two $\{Mo_3\}$ units where the Mo–Mo bonds are contracted to some 2.61 Å, while the Mo···Mo distances between triads are 3.31 Å. In an analogous structure, in the absence of a central oxo ligand, the terminal and the bridging oxo units have been formally exchanged with methoxo ligands formally leading to $[Nb_6(OCH_3)_{18}]^{2-}$.[120] The latter structure exhibits six Nb centres in an octahedral arrangement with crystallographic Nb–Nb bond lengths in the range of 2.87 to 2.88 Å. The authors have proposed that the bonding in $[Nb_6(OCH_3)_{18}]^{2-}$ arises from the six-centre two-electron bonds.[120] Similar bonding arrangements are prevalent in the hexanuclear $\{Ce_6O_8\}$-cores, which show spherical aromatic interactions of f-orbitals,[121] and within the hexaargentum clusters discussed in section 4 of this article. All of the latter species lack central guest ligands, such as the μ_6-O ligand that is present in the classical Lindqvist. It appears that the

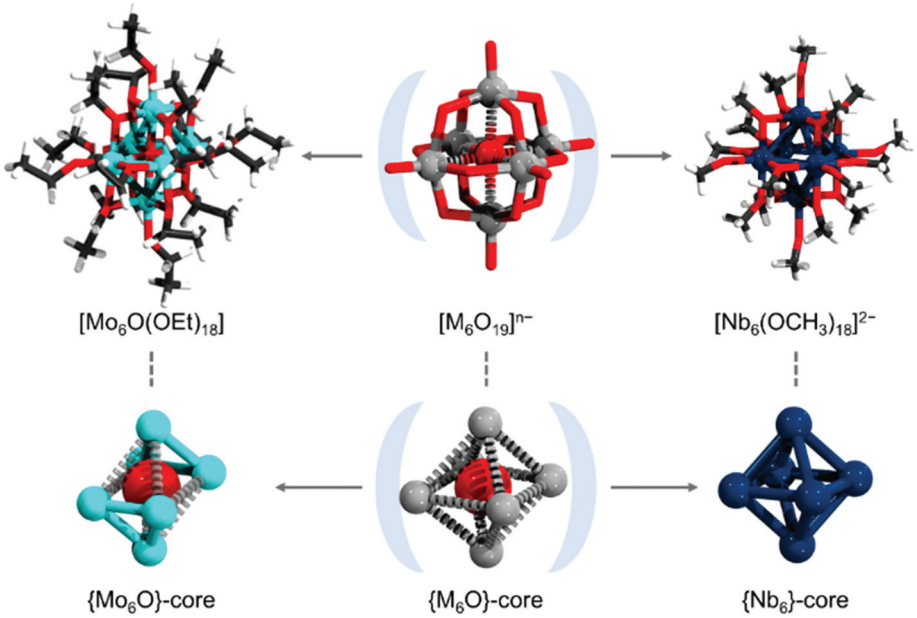

Fig. 8 Ball-and-stick representation of the classical $[M_6O_{19}]^{n-}$ structure (top centre) and the derived alkoxo hexamolybdate (top left) and hexaniobate (top right) and their respective cores are shown in the bottom row. Colour code: M = grey, Mo = cyan, Nb = dark teal, O = red, C = black and H = white spheres.

absence of the oxo ligand can enable bonding between all six centres, while its presence may lead to the formation of two separate triangular cluster type arrangements.

3. Homometallic metal–metal bonds stabilised by lacunary polyoxometalates

Homometallic bonds, especially between d-block centres, are very classical and represent textbook examples in inorganic chemistry.[108] These types of metal–metal bonds form as a result of the interaction of the M-centred s, p and d type orbitals, which in the case of M_2 molecules form pairs of metal-based bonding (σ, π, δ) and antibonding orbitals (σ*, π*, δ*). Local symmetry and the nature of the binding ligands influence the splitting and the relative energies of the molecular orbitals (classical diagram in Fig. 9a).[122] Electron population or de-population of orbitals can introduce configurational changes, which can be of interest in catalysis.[23] In this case, the combination of bimetallic d-block metal–metal bonds with POMs (*i.e.*, lacunary polytungstates) offers a possibility for the stabilisation of the system, high solubility of such complexes in water, and broader electrochemical capability due to the reduction of the W-addenda centres. The highest occupied molecular orbitals in these systems are typically associated with the heterometallic M–M bonded moiety, while the LUMOs are associated with the tungsten centres from the lacunary unit. Electron excitations normally can promote electron density from the heterometallic M–M bond to the POM, thus acting as all inorganic donor–acceptor systems.

Generation of metal–metal bonded POMs can be achieved electrosynthetically, starting with functional structures that do not exhibit metal–metal bonds in their ground state. An example of this is the diplatinate complex $[Pt_2^{II}(PW_{11}O_{39})_2]^{10-}$ anion where two Pt^{II} centres bridge two tetradentate $[PW_{11}O_{39}]^{7-}$ ligands. The $[Pt_2^{II}(PW_{11}O_{39})_2]^{10-}$ polyanions are formed under mildly acidic conditions (pH 3.5) by a reaction of α-$[PW_{11}O_{39}]^{7-}$ salts with K_2PtCl_4 in a molar ratio of 1 : 3. These POMs show short $Pt^{II}\cdots Pt^{II}$ contacts (XRD = 3.012, DFT = 3.14 Å) but an absence of metal–metal bonding. Following a projection of the highest occupied molecular orbital, it was observed that the two Pt^{II} units with a local d^8 configuration exhibit two axial d_{z^2}-like orbitals separated with a node, which is reminiscent of the σ*-like molecular orbital. Removal of two electrons from this orbital (Fig. 9a) is expected to generate Pt^{III} species with a d^7 electronic configuration, which can interact and produce a bond order. For platinum, the d^8 to d^7 change in the electronic configuration also changes the geometrical structure, that is, from square planar to square pyramidal. By decreasing the charge of the POM species and by modelling of two aqua ligands along the Pt–Pt axis, the polyanion $[Pt_2^{III}(H_2O)_2(PW_{11}O_{39})_2]^{8-}$ was derived. In the latter polyanion, the DFT calculated distance between the Pt^{III} (*i.e.*, d^7) centres is 2.64 Å, and the HOMO exhibited δ*-like character, which suggests the formation of a Pt–Pt bond (Fig. 9b). Based on time-dependent DFT, it has been showcased that both complexes exhibit significantly different UV-Vis spectral absorptions associated with a stark colour change. Using cyclic voltammetry and UV-Vis analysis, it has been showcased that the generation of the Pt^{III} derivatives is electrochemically revers-

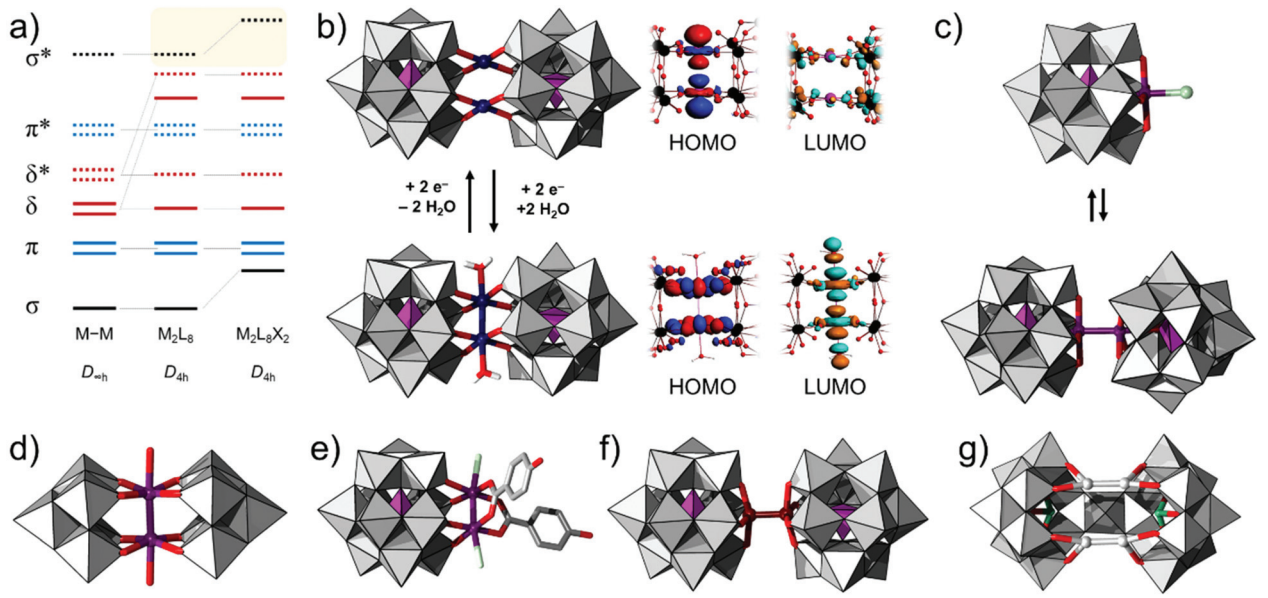

Fig. 9 (a) Schematic representation of the molecular bonding diagram describing M–M bonding in d-block complexes (redrawn from ref. 122). Combined ball-and-stick and polyhedral representation of (b) $[Pt_2^{II}(PW_{11}O_{39})_2]^{10-}$ (top row) and the two-electron oxidised $[Pt_2^{III}(H_2O)_2(PW_{11}O_{39})_2]^{8-}$ (bottom row); (c) $[PW_{11}O_{39}Rh^{III}Cl]^{5-}$ (top row) and $[(PW_{11}O_{39}Rh^{II})_2]^{10-}$ (bottom row); (d) $[PW_{11}O_{39}Rh_2(O_2CC_6H_4OH)_2Cl_2]^{7-}$; (e) $[(W_5O_{18})_2Rh_2(H_2O)_2]^{8-}$; (f) $[Re_2^{III}(PW_{11}O_{39})_2]^{8-}$; (g) $[(Hg_2)_2WO(H_2O)(AsW_9O_{33})_2]^{10-}$. Colour code: {$WO_6$} = grey octahedra, {$PO_4$} = purple tetrahedra, O = red, H = white, C = black, Pt = dark blue, Hg = white, Rh = purple, Re = brown, and Cl = light green spheres.

ible and associated solely with the formation of the Pt–Pt bond.[80]

Prior to this work, Pope and coworkers used electrosynthesis to produce Rh–Rh bonded POM species. By careful preparation, pH adjustment, and hydrothermal treatment of aqueous solutions containing phosphotungstic acid and $RhCl_3{\cdot}xH_2O$, Pope and coworkers have synthesised the monomeric $[PW_{11}O_{39}Rh^{III}Cl]^{5-}$ polyanion.[123] The latter polyanion has been subsequently electrochemically reduced at −0.52 V effectively accumulating 1 electron per kegginoid, leading to the formation of $[(PW_{11}O_{39}Rh^{II})_2]^{10-}$ species. The electrosynthetic reaction is followed by stark changes in colour (from orange to dark red). The isolated product has been characterised, and on this basis, XRD has shown Rh–Rh bonds of 2.52 Å (Fig. 9c). The deep red colouring of this POM also indicates the relatively low energy transition between the occupied and the unoccupied orbitals. UV-vis spectroscopy shows an absorption at 720 nm, which is attributed to the Rh–Rh-based $\pi^* \rightarrow \sigma^*$ transitions. The polyanion $[(PW_{11}O_{39}Rh^{II})_2]^{10-}$ can be re-oxidised by air, Br_2, and hypochlorite to return to the monomeric derivative $[PW_{11}O_{39}RhL]^{5-}$ where L = OH_2, Br and Cl.

A different arrangement of the Rh^{II} centres has been established by Sokolov and coworkers who reported the polyanion $[(W_5O_{18})_2Rh_2(H_2O)_2]^{8-}$ (Fig. 9d). Instead of electrosynthesis, this group has introduced $SnCl_2{\cdot}2H_2O$ for *in situ* generation of $\{Rh_2\}^{4+}$ species starting from the $RhCl_3$ precursor. The $\{Rh_2\}^{4+}$ links to two *in situ* generated lacunary $\{W_5O_{18}\}$ units. In $[(W_5O_{18})_2Rh_2(H_2O)_2]^{8-}$, each Rh^{II} centre links to two oxo groups of each $\{W_5O_{18}\}$ unit, which in a way is similar to the connectivity in the $[Pt_2^{III}(H_2O)_2(PW_{11}O_{39})_2]^{8-}$ model (*vide supra*). Axially the Rh^{II} centres bind to two aqua ligands, and they exhibit crystallographic Rh–Rh bond lengths in the range of 2.56 Å to 2.58 Å.[124]

Paddlewheel compounds with pre-existing Rh–Rh bonds such as $Rh_2(O_2CR)_4$ can be reacted hydrothermally with the monolacunary $[PW_{11}O_{39}]^{7-}$ leading to a variety of $[PW_{11}O_{39}Rh_2(RCOO)_2L_2]^{n-}$ derivatives where R = CH_3, L = DMSO, n = 5 and where R = CH_3, CH_2Cl, CH_2OH, C_3H_7, and *o*-/*p*-C_6H_4OH; L = Cl; and n = 7 (see an example in Fig. 9e).[125,126] The Rh–Rh bonds in these POMs are somewhat longer than those in the starting paddlewheel compounds. For instance, the length of the Rh–Rh bond in $[(PW_{11}O_{39}\{Rh_2(CH_3COO)_2(dmso)_2\}]^{5-}$ is 2.53 Å, and it is some 0.12 Å longer than that in $Rh_2(OAc)_4(dmso)_2$.[127] The stretches introduced in the Rh–Rh bonds by the R groups are minor (*e.g.*, 2.51 Å for R = *p*-C_6H_4OH to 2.52 Å for R = Pr^n). It has been proposed that the lacunary POM first binds axially to the rhodium paddlewheel, and then subsequently, it expels the carboxylate ligands. Once $[PW_{11}O_{39}Rh_2(RCOO)_2L_2]^{n-}$ is formed, the axial sites appear relatively inaccessible for further binding by bulky and lacunary POMs. However, the axial sites are still accessible for various (bio)organic ligands such as cysteine, methionine, and isonicotinic acid. Based on multinuclear NMR studies, it was shown that $[PW_{11}O_{39}Rh_2(RCOO)_2L_2]^{n-}$ has excellent solution stability in the pH range of pH 7–8.5. Inspired by the unusual structure and POM stability, the Cox group has reproduced $[(PW_{11}O_{39}\{Rh_2(CH_3COO)_2(dmso)_2\}]^{5-}$ and has applied it for the electrocatalytic oxidation of L-Met, L-cystine, and As(III) over a broad pH range.[128] This group has noted that POM fragments are likely to withdraw the electron density from the active di-rhodium site, making the material a donor–acceptor system. Similarly, the latter POM has been utilised to prepare carbon-composite electrodes that act as an amperometric detector. The Cox group also claimed to have synthesised the Rh–Rh containing derivative $[P_2Mo_{17}O_{39}\{Rh_2(O_2CCH_3)_2\}]^{8-}$; however, the formation of such a POM has been established mainly based on CV.[129] The latter POM has been claimed to be useful in the preparation of electrodes that reduce nitrite;[129] that oxidise arsenite,[129] phosphatidylcholines,[130] and methionine;[131] and that can sense bromate.[131]

Using the direct insertion strategy, Sokolov and coworkers have reported the di-rhenium complex $[Re_2^{III}(PW_{11}O_{39})_2]^{8-}$ exhibiting short Re–Re quadrupolar bonds with a distance of only 2.25 Å (Fig. 9f).[132] This POM has been obtained by the reaction of $[Cl_4Re{-}ReCl_4]^{2-}$ with $[PW_{11}O_{39}]^{7-}$ in highly acidic aqueous media (pH = 1), and it has been characterised based on X-ray diffraction crystallography, IR, and electrospray ionisation mass spectrometry. The high bond order in Re–Re derives from the formation of the $\sigma^2\pi^4\delta^2$ bonding configuration. Based on DFT, Chun-Guang Liu could confirm the bond configuration in the latter POM.[133] By studying the geometries of different $[Re_2^{III}(XW_{11}O_{39})_2]^{n-}$ where X = Al, Si, P, and S, it was found that the length of Re–Re bonds can minorly be influenced by the charge of the X centre that is for $X = Al^{III}$ (2.35 Å) > Si^{IV} (2.31 Å) > P^{V} (2.28 Å) > S^{VI} (2.26 Å). One- and two-electron reductions of $[Re_2^{III}(PW_{11}O_{39})_2]^{8-}$ led to the population of the antibonding δ* orbital, however, as the latter orbital is only weakly antibonding, its reduction does not lead to dissociation of the compound. Similarly, the excited state geometry corresponding to a transfer from the δ orbital to the antibonding δ* orbital retains the overall structure intact. Interestingly, the reductions in $[Re_2^{III}(PW_{11}O_{39})_2]^{8-}$ are also delocalized over the addenda tungsten centres.

Incorporation of Hg^{I}–Hg^{I} has been successfully achieved by the Jeannin group, who, by the reaction of sodium tungstate, diarsenic trioxide, and mercurous nitrate in water (pH 4) have isolated the clam-shaped polyanion $[(Hg_2)_2WO(H_2O)(AsW_9O_{33})_2]^{10-}$ (Fig. 9g).[134] In the latter polyanion, two *in situ* formed trilacunary $\{AsW_9O_{33}\}$ units are joined by a single $\{WO_6\}$ octahedron. Each Hg_2^{2+} subunit bridges the $\{AsW_9O_{33}\}$ units *via* two pairs of Hg–O bonds. In this orientation, the four mercury centres lie on the same plane and define the vertices of the virtual rectangle. The length of the Hg–Hg bonds is 2.55 Å. In contrast, the distance between the Hg^{I} neighbouring and non-bonded Hg centres is 3.66 Å. As the four Hg^{I} centres of each $[(Hg_2)_2WO(H_2O)(AsW_9O_{33})_2]^{10-}$ point towards the exterior of the structure, in the solid-state, the latter polyanion is found to pack as dimers with interatomic $Hg^{I}\cdots Hg^{I}$ distances of some 3.30 Å. This arrangement is owing to the prevalence of a close mercurophilic interaction.[135]

4. Heterometallic metal–metal bonds stabilised by lacunary polyoxometalates

In the late 1970s and early 1980s, Du Pont's industrial research chemist Walter H. Knoth Jr. excelled in integrating many different p-d based moieties (*e.g.*, Sn–Fe, Sn–Co, Sn–Pt, Ge–Fe, Ge–Co, *etc.*) functionalised by a diversity of coordination ligands and the d-block metal terminal. Many of these compounds were originally formed in water by reacting a preformed organometallic unit with monolacunary polytungstates.[44] Although we are currently unaware of any published application of these materials, in the original patent work, Knoth has claimed that these materials "have outstanding utility as catalysts for the oligomerization of terephthalic acid with ethylene glycol", that they are useful for the "isomerization of 1-butene" and for the "dehydration of 2-butanol and subsequent isomerization of the -butene occurred".[44] It is also noteworthy to mention that many of these discoveries took place shortly prior to the retirement of Knoth.[136]

The most archetypical example is Knoth's $[Cp(CO)_2Fe(SnSiW_{11}O_{39})]^{5-}$ (where Cp = C_5H_5) which consists of a {Cp$(CO)_2$Fe–Sn} moiety anchored on a monolacunary α-$[SiW_{11}O_{39}]^{8-}$ (see Fig. 10a). In Knoth's approach, the heterometallic p-d based moiety is already included within the precursor and is thus transferred in the final POM. On the other hand, in 1987, Pope and coworkers developed a slightly different approach leading to $[Cp(CO)_2Fe(SnSiW_{11}O_{39})]^{5-}$; however, the heterometallic unit is formed in the last step of the synthesis.[46] Therefore, Pope's approach relies on the use of tin(II) substituted kegginoid α-$[Sn^{II}SiW_{11}O_{39}]^{6-}$, however it is not a necessarily more synthetically facile strategy considering that α-$[Sn^{II}SiW^{VI}_{11}O_{39}]^{6-}$ is topologically sensitive and can interconvert to α-$[HO–Sn^{IV}SiW^{V}_{2}W^{VI}_{9}O_{39}]^{6-}$.[46] In the absence of crystallographic evidence, the particular structure was determined using ^{119}Sn NMR spectroscopy and IR that suggested integration of the tin(II) centre with the POM framework and the presence of the respective functional groups. Using the same overall approach, Knoth reported a series of monolacunary $[SiMo_{11}O_{39}]^{8-}$ and $[XW_{11}O_{39}]^{n-}$ (X/n = Si/8, Ge/8, Co/10, P/7) compounds functionalised by Sn–M′ bonds, where M = Fe, Co, Ni, Pt, Mo, W, Ir, Rh, Re, and Ru.[44]

Knoth is one of the first researchers who realised the potential of POMs to undergo post-modification.[62] An important example would be substitution of a single carbonyl ligand with $\{Sn^{II}O_3\}$ in $[(OC)_3Co(–SnPW_{11}O_{39})_2]^{9-}$ and its further reaction with monlacunary α-$[SiW_{11}O_{39}]^{8-}$ in aqueous media (pH 5) to form a bimodular $[(OC)_3Co(–SnPW_{11}O_{39})Sn(SiW_{11}O_{39})]^{10-}$ unit (Fig. 10b). Similar post-synthetic properties were also reported for other complexes, leading to $[(NO)(CO)_2Fe(SnSiW_{11}O_{39})_2]^{11-}$ and $[(\pi\text{-}C_3H_5)Pd(SnSiW_{11}O_{39})_2]^{11-}$.

Knoth has also demonstrated that insertion of multiple Sn–Fe moieties can be achieved when instead of monolacunary POMs, one uses simple building blocks (*e.g.*, WO_4^{2-} and PO_4^{3-}) or trilacunary species (*e.g.*, A-α-$[PW_9O_{34}]^{9-}$). The reaction of simple building blocks and $Cp(CO)_2Fe–SnCl_3$ in aqueous media (pH 8.0–8.6) leads to the formation of $[(CpFe(CO)_2Sn)_2PW_{10}O_{38}]^{5-}$ polyanions, which would be expected to exist in the form of multiple configurational isomers.

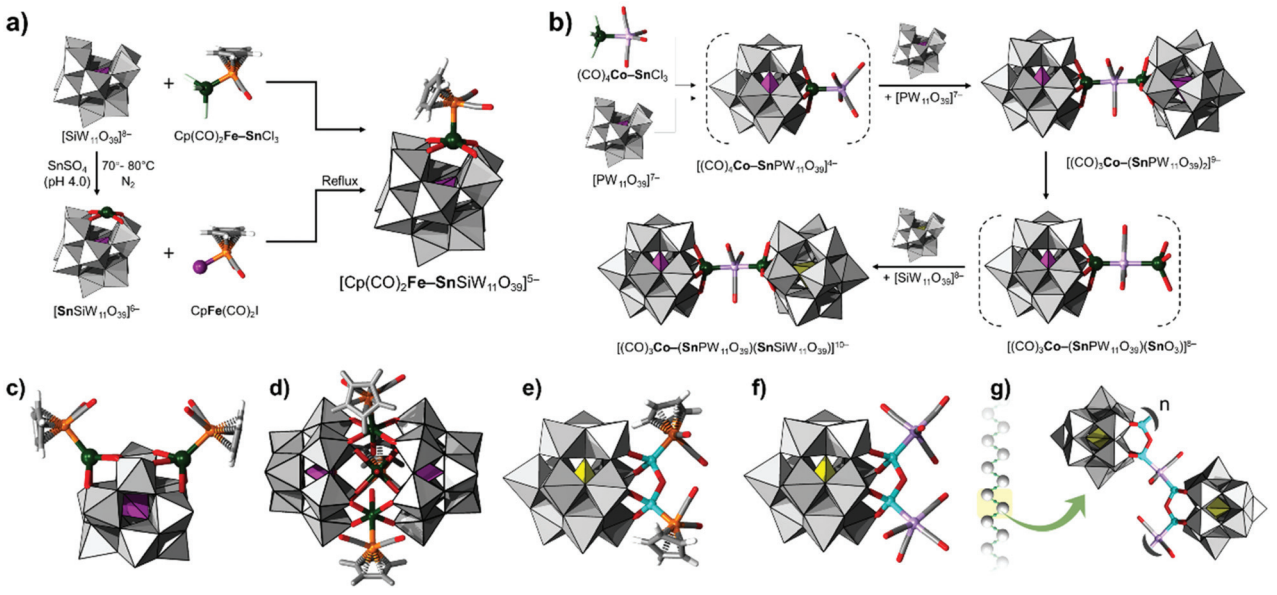

Fig. 10 Combined ball-and-stick representation of Knoth's proposed structural models, featuring: (a) scheme of insertion of a single Sn–Fe functionality following Knoth's (top row) and Pope's (bottom row) routes; (b) scheme of functionalisation of monolacunary $[PW_{11}O_{39}]^{7-}$ with {Co–Sn} moieties and its further dimerisation; (c) $[(CpFe(CO)_2Sn)_2PW_{10}O_{38}]^{5-}$; (d) $[(Cp(CO)_2Fe–Sn)_3(PW_9O_{34})_2]^{9-}$; (e) $[(CpFe(CO)_2Sn)_2W_{10}PO_{38}]^{5-}$; (f) $[(CO)_4Co–Ge]_2OSiW_{11}O_{39}]$; and (g) $\{[O(CO)_3Co–Ge]_2(SiW_{11}O_{39})_2]^{5-}\}_n$. Colour code: {$WO_6$} = grey octahedra, {$SiO_4$}/{$PO_4$} = yellow/purple tetrahedra, C = black, O = red, H = white, Fe = orange, Sn = dark green, Co = light violet, Ge = light cyan, I = purple, and Cl = light green spheres.

However, based on ^{31}P NMR showing a single signal and five, all equally intense, ^{183}W NMR signals, it was concluded that the formed POM likely exists in a 1,4-substituted conformation, exhibiting an overall C_2 symmetry point group (Fig. 10c).[137] On the other hand, reactions of trilacunary $[PW_9O_{34}]^{9-}$ with $Cp(CO)_2Fe–SnCl_3$ at pH 5.2 have led to a new formulation revealing a single ^{31}P NMR signal and two very broad lines in 1 : 2 ratio in the ^{183}W NMR spectrum. With consideration of the NMR data, IR, and elemental analysis, Knoth proposed that the sandwich-type structure $[(Cp(CO)_2Fe–Sn)_3(PW_9O_{34})_2]^{9-}$ would be a reasonable synthetic outcome (see Fig. 10d).[138] The proposed model is not entirely unusual considering that similar sandwich assemblies have been reported later for different organotin-containing POMs.[139–141] According to Knoth's observations, $[(Cp(CO)_2Fe–Sn)_3(PW_9O_{34})_2]^{9-}$ may have limited pH and thermal stability to some extent as it converts into simpler kegginoidal species.

In addition to Sn–M bonds, Knoth also reported insertions of handle-like $\{Ge_2O\}$ units within the POMs' lacunary cavity. The germanium sites can be coordinated with Ge–M bonds where M = Fe or Co. Particular examples are $[((C_5H_5)(CO)_2FeGe)_2O(SiW_{11}O_{39})]^{8-}$ (Fig. 10e) and $[((CO)_4CoGe)_2O(SiW_{11}O_{39})]^{8-}$ (Fig. 10f) which are obtained by reactions of $[SiW_{11}O_{39}]^{8-}$ with $(C_5H_5)(CO)_2Fe–GeCl_3$ and $(CO)_4Co–GeCl_3$, respectively.[142] Knoth also reported that the $[((CO)_4CoGe)_2O(SiW_{11}O_{39})]^{8-}$ polyanion undergoes formal $\{Co(CO)_5\}$ loss allowing it to polymerise into $\{[[(CO)_3Co–Ge]_2OSiW_{11}O_{39}]^{5-}\}_n$ (Fig. 10g) species with a molecular weight of *ca.* 1000 kDa as resolved based on solution light scattering in DMS.[45]

The main criticism of the work of Knoth is that most of the reported complexes are logically deduced based on spectroscopic and elemental data; however, they still lack substantial structural elucidation. The heterometallic metal(loid)–metal bonds in these compounds allow the coupling of electron-rich (donor) groups with highly oxidised POMs that can readily be reduced, that is, act as an electron acceptor group. The short separation from the 3d group metal to the POM surface may be further interesting for proton-coupled (photo)electrocatalysis considering that the highly negative POM surface commonly interacts with protons. This property of the POM surface has been recently demonstrated to be essential when designing organometallic coordination complexes such as $[\alpha\text{-}H_2PW_{11}O_{39}\{Rh^{III}Cp^*(OH_2)\}]^{3-}$ that can serve in catalytic CO_2 reduction.[143]

5. Cluster stabilisation and other metal–metal bonds in POMs

Heterometal-rich POMs can engage in encapsulation or nanoconfinement of cations and clusters.[144] With the help of POMs, nanoconfinement may aid the formation and the stabilisation of metal nanoclusters, metal triads and other forms of highly reduced clusters.

In section 3 we have discussed the coordination of POMs to instances of pairs of d-block heterometallic centres connected *via* metal–metal bonds. Among the different d-block elements, interactions with low valent silver–silver bonded units would not be expected. The reason is that silver is well-known to build nanoclusters with relevance in sensing, biolabeling, and catalysis.[145,146] The silver clusters typically are very susceptible and reactive to molecular oxygen, and thus to be protected, they typically involve organic molecules as stabilising ligands.[145] Lacunary POMs normally would not be expected to bind successfully to silver nanoclusters without risk of oxidizing them. However, once achieved, such systems may, similar to the other systems described in section 3, act as all-inorganic donor–acceptor systems.

In 2013, the group of Mizuno discovered that reactions of γ-$[SiW_{10}O_{36}]^{8-}$ and silver(I) acetate in acetone media performed in the presence of reducing dimethylphenylsilane lead to the formation of sandwich-type $[Ag_6(\gamma\text{-}H_2SiW_{10}O_{36})_2]^{8-}$ (Fig. 11a).[147] In the sandwich structure, a central octahedral $[Ag_6]^{4+}$ cluster has two valence electrons that are delocalised over the six Ag centres. Simultaneously, the two lacunary γ-$[SiW_{10}O_{36}]^{8-}$ units stabilise the cluster from the outside *via* Ag–O–W. This strategy was recently extended to the preparation of $\{Ag_7\}^{5+}$,[148] and $\{Ag_{27}\}^{17+}$ complexes (Fig. 11a).[149] The preparation of the latter structures does depend on direct reduction with dimethylphenylsilane, but it is believed that small water impurities may be causing the reduction over a prolonged time period. These clusters are prepared by the use of the trilacunary $[SiW_9O_{34}]^{10-}$ and its alkoxo substituted $[SiW_9O_{28}(OCH_3)_6]^{4-}$ derivative. For the stabilisation of $\{Ag_7\}^{5+}$, the lacunary $[SiW_9O_{34}]^{10-}$ trimerises into a cyclic $[Si_3W_{27}O_{96}]^{18-}$ polyanion where the $\{Ag_7\}^{5+}$ cluster is encapsulated in its cavity.[148] The softer alkoxo substituted trilacunary POM causes an *in situ* dimerization of the $[SiW_9O_{34}]^{10-}$ lacunary POMs to dimeric $[Si_2W_{18}O_{66}]^{16-}$ units. Three $[Si_2W_{18}O_{66}]^{16-}$ units are then involved in the stabilisation of the $\{Ag_{27}\}^{17+}$ cluster.[149] Within the silver clusters, the delocalised electrons cause metal–metal bonding, and these electrons normally constitute the HOMO. The LUMO in these systems is delocalised over the polytungstate unit. Therefore the UV-Vis absorptions normally correspond to the transfer of the electron density from the cluster to the lacunary POM, which in essence represents a donor–acceptor system.[147–149]

In 2011, Xue and coworkers reported that the reaction of As_2O_3 with heptamolybdate (*i.e.* $[Mo_7O_{24}]^{6-}$) and silver cations in neutral aqueous media leads to the formation of an $[(AgAs_2O_6)Mo_{15}O_{48}]^{11-}$ polyanion (Fig. 11b).[150] The latter polyanion has an overall C_{3v} point group symmetry. This POM can be described as a host–guest system comprising an $[O_3As^{III}–Ag^{I}–As^{III}O_3]^{5-}$ guest moiety with an idealised D_{3h} symmetry encapsulated within a hexagonally prismatic $[Mo_{15}O_{48}]^{6-}$ host (Fig. 11b). The negatively charged $[Mo_{15}O_{48}]^{6-}$ shell has a surplus of more than three oxo ligands per addenda centre, which indicates that it is unsaturated and may be further reactive. Considering the overall environment, the guest unit $[O_3As^{III}–Ag^{I}–As^{III}O_3]^{5-}$ exhibits two inequivalent $As^{III}–Ag^{I}$ bonds with lengths of 2.56 Å and 2.62 Å. These bond lengths are within the typical range for As–Ag bonds as measured in

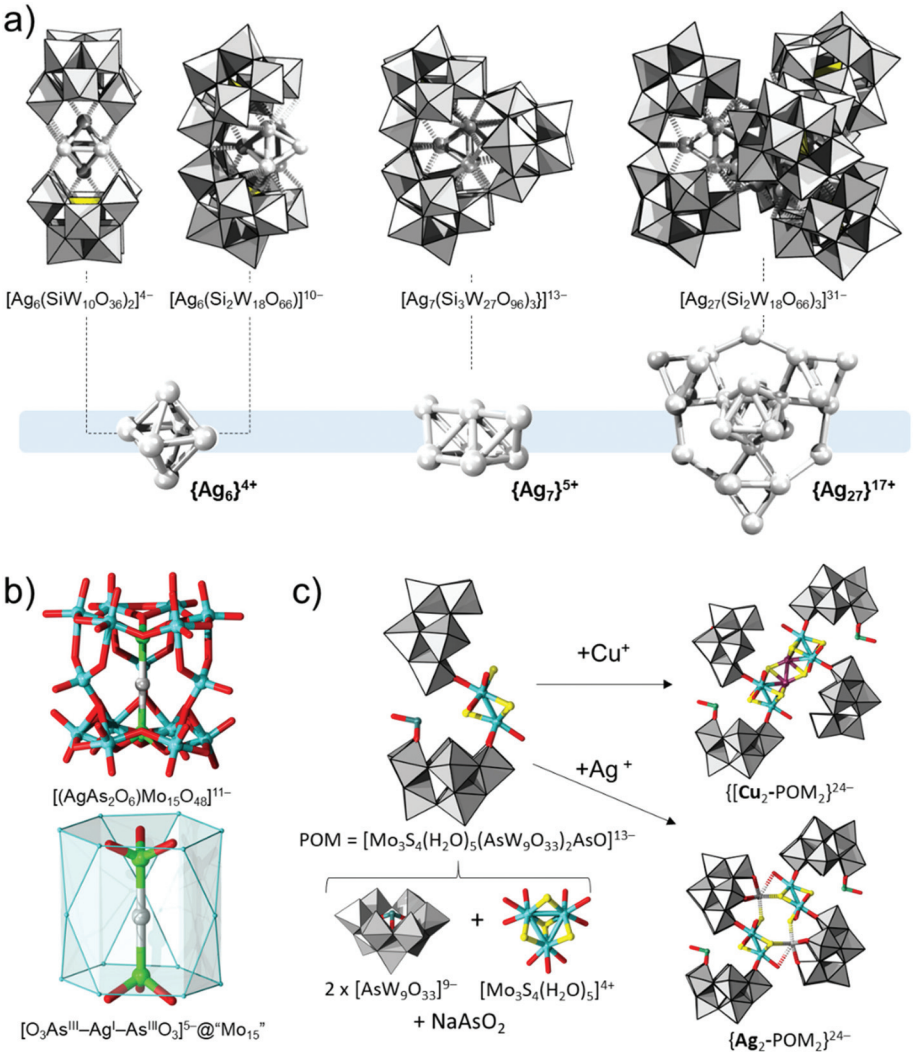

Fig. 11 Combined ball-and-stick and polyhedral representation of (a) different di- and trilacunary polytungstates incorporating silver cluster cores; (b) $[(AgAs_2O_6)Mo_{15}O_{48}]^{11-}$ polyanion (top) and the $[O_3As^{III}–Ag^{I}–As^{III}O_3]^{5-}$ moiety within the distorted hexagonal prismatic "Mo_{15}" = $[Mo_{15}O_{48}]^{6-}$ host (bottom); (c) Schematic representation of the integration of $[AsW_9O_{33}]^{9-}$ with $[Mo_3S_4(H_2O)_5]^{4+}$ and the subsequent oligomerisation due to Ag–Ag and Cu–Cu bonds. Colour code: O = red, Mo = cyan, As = green and Ag = grey spheres, Cu = purple, S = yellow spheres and $\{MoO_6\}$ = grey polyhedra and $\{Mo_{15}\}$ = light blue prism.

relevant solid compounds.[151] Irradiation of $[(AgAs_2O_6)Mo_{15}O_{48}]^{11-}$ with light at λ = 490 nm produces an intense luminescence peak at 496 nm, which is assigned to the d–d electronic transition at the Ag^I centre.[150]

Cuboidal $\{Mo_4S_4(H_2O)_{12}\}^{4+}$ clusters have been long investigated, and their fragmented $\{Mo_3S_4\}$ derivatives have been effectively incorporated into many POMs.[48,56] The polyanion $[Mo_3S_4(H_2O)_5(AsW_9O_{33})_2AsO]^{13-}$ has been obtained as a result of integration between two $\{AsW_9O_{33}\}$ and $\{Mo_3S_4\}$ units and a single {AsO}. In the solid-state, the former polyanion can dimerise due to ionic bridging with two K^+ centres binding at the terminal oxo sites of the lacunary unit. When M = Ag^+ or Cu^+ cations are inserted, dimeric $\{[MMo_3S_4(H_2O)_5(AsW_9O_{33})_2AsO]_2\}^{24-}$ assemblies form; however, two structurally different archetypes are obtained (Fig. 11c).[152] In the solid-state, the silver cations replace potassium, whilst the Cu^+ centres participate in the formation of a cuboidal $\{CuMo_3S_4\}$ unit and enforce the dimerisation *via* Cu–Cu bond bridges of 2.34 Å. Similarly, $[(AsW_9O_{33})_4\{M'Mo_3^{VI}S_4(H_2O)_5\}_2]^{28-}$ (M′ = Pd or Ni) derivatives have been prepared in reactions of $[M'Mo_3S_4(H_2O)_9Cl]^{3+}$ with $[AsW_9O_{33}]^{9-}$.[153] In the latter polyanions, the Pd–Pd and Ni–Ni bonding distances are 2.74 Å and 2.55 Å, respectively, while within the cuboidal units, the Mo–Mo, Mo–Pd, and Mo–Ni distances are in the range of 2.73–2.78 Å, 2.73–2.85 Å and 2.63–2.70 Å, respectively. Solution characterisation based on UV-vis and ^{183}W NMR spectroscopy revealed moderate stability of the dimeric structures, which could be disrupted by titration with iodide or pyridine due to the dissociation of the bridging M′–M′ bonds and coordination of the ligands. Cyclic voltammetry showed irreversible redox processes where the peak potentials were shown to be dependent upon the

ionic charge of the POM. In the Pd case, the cyclic voltammetry was shown to be consistent with the deposition and oxidation of palladium at the electrode.

6. Summary and outlook

The current review does not dismiss Cotton's traditional distinction between metal clusters and fully oxydised POMs on the basis of metal–metal bonds (Figure 1). However, the review points out that there is an undeniable set of POMs with metal–metal bonding in the core of their constitution that places such materials at the interface between the two traditional categories. In comparison to other subdomains of POMs (*e.g.*, hybrid POMs), the set of metal–metal bonded POMs currently features only a modest number of structures; however, the structures provide an unprecedented versatility in terms of bonding chemistry and electronic structure that is probably unrivalled by other historically more intensely researched areas of POM chemistry.

In the case of homometallic bonding between addenda POM centres, the starting metal–metal bonded solution species appear as key precursors in programmable self-assembly of cage-like nanoscale systems. The programmable self-assembly using such building blocks shows potential to be further extended, leading to hybrid materials where the metal–metal bonded POMs can serve as secondary building units or even as hybrid platforms for post-synthetic modifications. Whether the high reductions in POMs are associated with an increase in metal–metal bonding is also dependent on the constituting element, the POM archetype and the redox state. For certain archetypes, symmetry breaks are inevitable, leading to localisation of the charge, which can also be limiting when considering applying certain POMs as extreme molecular supercapacitors. However, this type of symmetry breaks and charge localisation also paves the way for the preparation of POMs bearing partially metal cluster-like features. As Xu has pointed out, such POMs may have a strong application as hydrogenation catalysts. The interplay of strain, symmetry, and covalent dynamics is also an important aspect of this set of compounds, which will be more closely followed theoretically in the near future. The formal exchange of oxo with alkoxo ligands was mentioned as a potential strategy to learn more about the evolution of the metal–metal bonds in some shared POM archetypes. With consideration of the advances in polyalkoxovanadate chemistry,[57] certain novel mixed metal hybrids of V/Mo and V/Nb may provide some interesting reactivities indeed and charge storing properties.

POMs that integrate metal–metal bonded functionalities pave the path for an interplay between the classical POM features (*e.g.*, multielectron reductions and surface Lewis basicity) and the metal–metal bonded functionality. This is most pronounced in section 3 where the chemistry of homometallic bonding between heterometals in POMs was discussed. Such materials clearly combine the properties of the metal–metal bonded unit and the polydentate aspects of the lacunary POM ligands. It is very unfortunate that this domain of chemistry has earned little attention in the past decades, exemplified with only several archetypes. However, with the emerging reports on the design of d-block heterobimetallic complexes[154,155] and their value in molecular catalysis, one can envision the potential of this area to flourish in the near future. Lacunary POMs as ligands can offer redox properties that are unmatched by organic ligands, a surface that can be protonated, excellent solubility in water and occasionally selective interactions with biomolecules. The number of discussed archetypes in this article certainly opens the possibility for structured *in silico* exploration of various heterobimetallic POM complexes, which can serve as a guide for the synthetic design of new POMs with tailored applications.

In the final sections, the article touched upon the exploration of the many examples of heterometallic bonds between combinations of d-block and p-block metals. Such combinations provide possibilities for shortening the path between potential chromophores and POMs which can be used for the rational design of functional donor–acceptor systems. The challenges in this chemistry that Knoth and Pope faced some four decades ago relate to their characterisation and description, which nowadays, with the modern analytical and computational techniques, may be more conveniently tackled. Among the remaining assemblies of POMs with different metal–metal bonds, the combination of silver clusters with lacunary polyoxotungstates provides an excellent platform for the design of all-inorganic donor–acceptor systems. A decade ago, this compatibility between lacunary POMs and metal clusters could not have been easily envisioned; however, it now encourages ambitious integration of POMs and metal clusters for the design of molecular junctions and even hybrid networks.

The author of the article believes that the outlined examples and chemistry can serve as a bridge between POMs, metal clusters and metal–metal complex chemistry and thus build upon talent and collaborations existing in different communities. The future evolution of the subject and its increase in complexity are necessary to establish ways towards metal–metal based POMtroncis. In addition to the close integration of theoretical and experimental techniques, this domain will likely benefit from the emerging digitalisation and knowledge engineering technologies that are gaining popularity in chemical nanotechnology.

Conflicts of interest

There are no conflicts to declare.

Acknowledgements

AK thanks the Alexander von Humboldt Foundation and Research Foundation Flanders (FWO) for postdoctoral fellowships. The projection of orbitals in figures was enabled using the Amsterdam Modelling Suite (https://www.scm.com/).

Notes and references

1 S. L. Sass, *The Substance of Civilization: Materials and Human History from the Stone Age to the Age of Silicon*, Skyhorse Publishing, 2011.
2 W. H. Brock, *Norton history of chemistry*, W.W. Norton & Co Inc, New York, NY, 1993.
3 N. Amzallag, *Am. J. Archaeol.*, 2009, 497–519.
4 M. Nicola, C. Mastrippolito and A. Masic, *Iron Oxides*, 2016, 545–566.
5 M. V. Orna, M. J. D. Low and N. S. Baer, *Stud. Conserv.*, 1980, **25**, 53–63.
6 A. Coccato, L. Moens and P. Vandenabeele, *Herit. Sci.*, 2017, **5**, 12.
7 R. G. Neville, *J. Chem. Educ.*, 1974, **51**, 428.
8 H. Cassebaum and J. A. Schufle, *J. Chem. Educ.*, 1975, **52**, 442.
9 R. Siegfried, *Osiris*, 1988, **4**, 34–50.
10 R. G. Arns, *Eng. Sci. Educ. J.*, 1998, **7**, 233–240.
11 L. Petti, N. Münzenrieder, C. Vogt, H. Faber, L. Büthe, G. Cantarella, F. Bottacchi, T. D. Anthopoulos and G. Tröster, *Appl. Phys. Rev.*, 2016, **3**, 21303.
12 D. Rotman, *We're not prepared for the End of Moore's Law.*, *MIT Technol. Rev.*, 2020.
13 H. N. Khan, D. A. Hounshell and E. R. H. Fuchs, *Nat. Electron.*, 2018, **1**, 14–21.
14 G. Aromí, D. Aguila, P. Gamez, F. Luis and O. Roubeau, *Chem. Soc. Rev.*, 2012, **41**, 537–546.
15 A. Gaita-Ariño, F. Luis, S. Hill and E. Coronado, *Nat. Chem.*, 2019, **11**, 301–309.
16 M. H. Chisholm and Lord Lewis of Newnham, *Biogr. Mem. Fellows R. Soc.*, 2008, **54**, 95–115.
17 M. T. Pope, *Heteropoly and Isopoly Oxometalates*, Springer-Verlag, Berlin, Heidelberg, 1983, vol. 8.
18 D.-L. Long, R. Tsunashima and L. Cronin, *Angew. Chem., Int. Ed.*, 2010, **49**, 1736–1758.
19 F. A. Cotton, N. F. Curtis, C. B. Harris, B. F. G. Johnson, S. J. Lippard, J. T. Mague, W. R. Robinson and J. S. Wood, *Science*, 1964, **145**, 1305–1307.
20 J. F. Berry and C. C. Lu, *Inorg. Chem.*, 2017, **56**, 7577–7581.
21 J. E. McGrady, in *Encyclopedia of Inorganic Chemistry*, ed. R. B. King, R. H. Crabtree, C. M. Lukehart, D. A. Atwood and R. A. Scott, Wiely, 2009.
22 J. E. McGrady, *Mol. Met. Bonds*, 2015, 1–22.
23 P. A. Lindahl, *J. Inorg. Biochem.*, 2012, **106**, 172–178.
24 V. P. Georgiev and J. E. McGrady, *J. Am. Chem. Soc.*, 2011, **133**, 12590–12599.
25 V. P. Georgiev and J. E. McGrady, *Inorg. Chem.*, 2010, **49**, 5591–5597.
26 A. Kondinski and T. N. Parac-Vogt, *Front. Chem.*, 2018, **6**, 346.
27 N. V. Izarova, M. T. Pope and U. Kortz, *Angew. Chem., Int. Ed.*, 2012, **51**, 9492–9510.
28 M. Nyman and P. C. Burns, *Chem. Soc. Rev.*, 2012, **41**, 7354–7367.
29 L. Vilà-Nadal, A. Rodríguez-Fortea, L.-K. Yan, E. F. Wilson, L. Cronin and J. M. Poblet, *Angew. Chem., Int. Ed.*, 2009, **48**, 5452–5456.
30 P. Yin, D. Li and T. Liu, *Chem. Soc. Rev.*, 2012, **41**, 7368–7383.
31 S.-S. Wang and G.-Y. Yang, *Chem. Rev.*, 2015, **115**, 4893–4962.
32 C. Streb, K. Kastner and J. Tucher, *Phys. Sci. Rev.*, 2019, **4**(6), 20170177.
33 J. M. Clemente-Juan, E. Coronado and A. Gaita-Ariño, *Chem. Soc. Rev.*, 2012, **41**, 7464–7478.
34 V. Das, R. Kaushik and F. Hussain, *Coord. Chem. Rev.*, 2020, **413**, 213271.
35 L. Chen, W.-L. Chen, X.-L. Wang, Y.-G. Li, Z.-M. Su and E.-B. Wang, *Chem. Soc. Rev.*, 2019, **48**, 260–284.
36 H. D. Pratt, N. S. Hudak, X. Fang and T. M. Anderson, *J. Power Sources*, 2013, **236**, 259–264.
37 B. Huang, D.-H. Yang and B.-H. Han, *J. Mater. Chem. A*, 2020, **8**, 4593–4628.
38 M. Anjass, G. A. Lowe and C. Streb, *Angew. Chem., Int. Ed.*, 2021, 7522–7532.
39 M. H. Anjass, M. Deisböck, S. Greiner, M. Fichtner and C. Streb, *ChemElectroChem*, 2019, **6**, 398–403.
40 X. Chen, Y. Zhou, V. A. L. Roy and S.-T. Han, *Adv. Mater.*, 2018, **30**, 1703950.
41 N. I. Gumerova and A. Rompel, *Nat. Rev. Chem.*, 2018, **2**, 112.
42 S.-C. Huang, C.-C. Lin, C.-W. Hu, Y.-F. Liao, T.-Y. Chen and H.-Y. Chen, *J. Power Sources*, 2019, **435**, 226702.
43 C.-C. Lin, C.-T. Hsu, W. Liu, S.-C. Huang, M.-H. Lin, U. Kortz, A. S. Mougharbel, T.-Y. Chen, C.-W. Hu, J.-F. Lee, C.-C. Wang, Y.-F. Liao, L.-J. Li, L. Li, S. Peng, U. Stimming and H.-Y. Chen, *ACS Appl. Mater. Interfaces*, 2020, **12**, 40296–40309.
44 W. H. Knoth, *US Patent*, 4196136A, 1980.
45 W. H. Knoth, *J. Am. Chem. Soc.*, 1979, **101**, 2211–2213.
46 G. S. Chorghade and M. T. Pope, *J. Am. Chem. Soc.*, 1987, **109**, 5134–5138.
47 P. Mialane, A. Dolbecq, L. Lisnard, A. Mallard, J. Marrot and F. Sécheresse, *Angew. Chem., Int. Ed.*, 2002, **41**, 2398–2401.
48 E. Cadot, M. N. Sokolov, V. P. Fedin, C. Simonnet-Jégat, S. Floquet and F. Sécheresse, *Chem. Soc. Rev.*, 2012, **41**, 7335–7353.
49 M. T. Pope and A. Muller, *Angew. Chem., Int. Ed. Engl.*, 1991, **30**, 34–48.
50 U. Kortz, A. Müller, J. van Slageren, J. Schnack, N. S. Dalal and M. Dressel, *Coord. Chem. Rev.*, 2009, **253**, 2315–2327.
51 A. Müller, E. Krickemeyer, H. Bögge, M. Schmidtmann and F. Peters, *Angew. Chem., Int. Ed.*, 1998, **37**, 3359–3363.
52 X. López, J. J. Carbó, C. Bo and J. M. Poblet, *Chem. Soc. Rev.*, 2012, **41**, 7537–7571.
53 D. M. P. Mingos, *Bonding and Charge Distribution in Polyoxometalates: A Bond Valence Approach*, Springer, Berlin, 1999.
54 L. R. Kazansky, in *Polyoxometalate Molecular Science*, Springer, 2003, pp. 175–209.
55 J. Zhang, F. Xiao, J. Hao and Y. Wei, *Dalton Trans.*, 2012, **41**, 3599–3615.
56 H. N. Miras, *Chem. – Eur. J.*, 2014, **20**, 10554–10560.

57 L. E. VanGelder, A. M. Kosswattaarachchi, P. L. Forrestel, T. R. Cook and E. M. Matson, *Chem. Sci.*, 2018, **9**, 1692–1699.
58 A. Misra, K. Kozma, C. Streb and M. Nyman, *Angew. Chem.*, 2020, **59**, 596–612.
59 C. Busche, L. Vilà-Nadal, J. Yan, H. N. Miras, D.-L. Long, V. P. Georgiev, A. Asenov, R. H. Pedersen, N. Gadegaard, M. M. Mirza, D. J. Paul, J. M. Poblet and L. Cronin, *Nature*, 2014, **515**, 545–549.
60 S. V. Krivovichev, *Angew. Chem., Int. Ed.*, 2014, **53**, 654–661.
61 C. Simms, A. Kondinski and T. N. Parac-Vogt, *Eur. J. Inorg. Chem.*, 2020, 2559–2572.
62 A. V. Anyushin, A. Kondinski and T. N. Parac-Vogt, *Chem. Soc. Rev.*, 2020, **49**, 382–432.
63 J. M. Poblet and X. López, in *Encyclopedia of Inorganic Chemistry*, ed. R. B. King, R. H. Crabtree, C. M. Lukehart, D. A. Atwood and R. A. Scott, 2009, pp. 453–466.
64 J. Tucher, Y. Wu, L. C. Nye, I. Ivanovic-Burmazovic, M. M. Khusniyarov and C. Streb, *Dalton Trans.*, 2012, **41**, 9938–9943.
65 Y. Bai, Y. Dou, L.-H. Xie, W. Rutledge, J.-R. Li and H.-C. Zhou, *Chem. Soc. Rev.*, 2016, **45**, 2327–2367.
66 H. G. T. Ly, G. Fu, A. Kondinski, B. Bueken, D. De Vos and T. N. Parac-Vogt, *J. Am. Chem. Soc.*, 2018, **140**, 6325–6335.
67 A. Kondinski, *Chem. Model.*, 2021, **16**, 39–71.
68 The reader should note that here one differentiates between the solution species that participate in the self-assembly of a POM structure and structural fragments that virtually constitute the POM topology. Ontologically, the fragments are connected to the solution species *via* the "derives from" relationship. The fragments are not necessarily "equivalent to" or "the same as" the solution species. For instance, a tetrahedral orthometalate may be the solution species $\{MO_4\}$, but the corresponding structural fragment may be the $\{MO_5\}$ square pyramidal unit.
69 A. Kondinski and K. Y. Monakhov, *Chem. – Eur. J.*, 2017, **23**, 7841–7852.
70 J. R. Winkler and H. B. Gray, in *Molecular Electronic Structures of Transition Metal Complexes I*, ed. D. M. P. Mingos, P. Day and J. P. Dahl, in Springer Berlin Heidelberg, Berlin, Heidelberg, 2012, pp. 17–28.
71 F. A. Cotton, *Acc. Chem. Res.*, 1969, **2**, 240–247.
72 C. Sharp, E. F. Hills and A. G. Sykes, *J. Chem. Soc., Dalton Trans.*, 1987, 2293–2297.
73 X. Huang, H.-J. Zhai, B. Kiran and L.-S. Wang, *Angew. Chem., Int. Ed.*, 2005, **44**, 7251–7254.
74 A. Bino, F. A. Cotton and Z. Dori, *J. Am. Chem. Soc.*, 1978, **100**, 5252–5253.
75 M. Segawa and Y. Sasaki, *J. Am. Chem. Soc.*, 1985, **107**, 5565–5566.
76 A. Müller, R. Jostes and F. A. Cotton, *Angew. Chem., Int. Ed. Engl.*, 1980, **19**, 875–882.
77 E. Benory, A. Bino, D. Gibson, F. A. Cotton and Z. Dori, *Inorg. Chim. Acta*, 1985, **99**, 137–142.
78 M. Pley and M. S. Wickleder, *Angew. Chem., Int. Ed.*, 2004, **43**, 4168–4170.
79 M. Pley and M. Wickleder, *Z. Naturforsch. B*, 2006, **61**, 912–915.
80 Z. Lin, N. V. Izarova, A. Kondinski, X. Xing, A. Haider, L. Fan, N. Vankova, T. Heine, B. Keita, J. Cao, C. Hu and U. Kortz, *Chem. – Eur. J.*, 2016, **22**, 5514–5519.
81 A. Kondinski, T. Heine and K. Y. Monakhov, *Inorg. Chem.*, 2016, **55**, 3777–3788.
82 L. C. W. Baker and J. S. Figgis, *J. Am. Chem. Soc.*, 1970, **92**, 3794–3797.
83 X. López and J. M. Poblet, *Inorg. Chem.*, 2004, **43**, 6863–6865.
84 F.-Q. Zhang, X.-M. Zhang, H.-S. Wu, Y.-W. Li and H. Jiao, *J. Phys. Chem. A*, 2007, **111**, 1683–1687.
85 E. Cadot, V. Béreau, B. Marg, S. Halut and F. Sécheresse, *Inorg. Chem.*, 1996, **35**, 3099–3106.
86 J. C. Kemmegne-Mbouguen, S. Floquet, D. Zang, A. Bonnefont, L. Ruhlmann, C. Simonnet-Jégat, X. López, M. Haouas and E. Cadot, *New J. Chem.*, 2019, **43**, 1146–1155.
87 K. Y. Monakhov, M. Moors and P. Kögerler, *Adv. Inorg. Chem.*, 2017, **69**, 251–286.
88 B. Nohra, H. El Moll, L. M. R. Albelo, P. Mialane, J. Marrot, C. Mellot-Draznieks, M. O'Keeffe, R. N. Biboum, J. Lemaire, B. Keita, L. Nadjo and A. Dolbecq, *J. Am. Chem. Soc.*, 2011, **133**, 13363–13374.
89 X.-X. Li, D. Zhao and S.-T. Zheng, *Coord. Chem. Rev.*, 2019, **397**, 220–240.
90 W. Cheng, F.-C. Shen, Y. Xue, X. Luo, M. Fang, Y.-Q. Lan and Y. Xu, *ACS Appl. Energy Mater.*, 2018, **1**, 4931–4938.
91 T. Iijima, T. Yamase, M. Tansho, T. Shimizu and K. Nishimura, *J. Phys. Chem. A*, 2014, **118**, 2431–2441.
92 A. I. Frenkel, S. C. Frankel and T. Liu, *Phys. Scr.*, 2005, 721.
93 D. Melgar, N. A. G. Bandeira and C. Bo, *Chem. – Eur. J.*, 2017, **23**, 5338–5344.
94 A. Müller, P. Kögerler and A. W. M. Dress, *Coord. Chem. Rev.*, 2001, **222**, 193–218.
95 A. Rezaeifard, R. Haddad, M. Jafarpour and M. Hakimi, *J. Am. Chem. Soc.*, 2013, **135**, 10036–10039.
96 N. Watfa, D. Melgar, M. Haouas, F. Taulelle, A. Hijazi, D. Naoufal, J. B. Avalos, S. Floquet, C. Bo and E. Cadot, *J. Am. Chem. Soc.*, 2015, **137**, 5845–5851.
97 Z. Lang, I. M. Gabas, X. López, A. Clotet, J. M. de la Fuente, S. G. Mitchell and J. M. Poblet, *New J. Chem.*, 2016, **40**, 1029–1038.
98 B. Keita, R. N. Biboum, I. M. Mbomekallé, S. Floquet, C. Simonnet-Jégat, E. Cadot, F. Miserque, P. Berthet and L. Nadjo, *J. Mater. Chem.*, 2008, **18**, 3196–3199.
99 M. J. Manos, J. D. Woollins, A. M. Z. Slawin and T. A. Kabanos, *Angew. Chem., Int. Ed.*, 2002, **41**, 2801–2805.
100 J. P. Launay, *J. Inorg. Nucl. Chem.*, 1976, **38**, 807–816.
101 S. P. E. Smith and J. B. Christian, *Electrochim. Acta*, 2008, **53**, 2994–3001.
102 K. Piepgrass and M. T. Pope, *J. Am. Chem. Soc.*, 1987, **109**, 1586–1587.
103 Y. Jeannin, J. P. Launay and M. A. S. Sedjadi, *Inorg. Chem.*, 1980, **19**, 2933–2935.
104 C. Boskovic, M. Sadek, R. T. C. Brownlee, A. M. Bond and A. G. Wedd, *J. Chem. Soc., Dalton Trans.*, 2001, 187–196.

105 M. H. Dickman, T. Ozeki, J. Evans, H. T. C. Rong, G. B. Jameson and M. T. Pope, *J. Chem. Soc., Dalton Trans.*, 2000, 149–154.
106 Y. Nishimoto, D. Yokogawa, H. Yoshikawa, K. Awaga and S. Irle, *J. Am. Chem. Soc.*, 2014, **136**, 9042–9052.
107 H. Wang, S. Hamanaka, Y. Nishimoto, S. Irle, T. Yokoyama, H. Yoshikawa and K. Awaga, *J. Am. Chem. Soc.*, 2012, **134**, 4918–4924.
108 F. A. Cotton, G. Wilkinson, C. A. Murillo, M. Bochmann and R. Grimes, *Advanced inorganic chemistry*, Wiley, New York, 1988, vol. 6.
109 W.-P. Chen, R.-L. Sang, Y. Wang and L. Xu, *Chem. Commun.*, 2013, **49**, 5883–5885.
110 F. A. Cotton, D. O. Marler and W. Schwotzer, *Inorg. Chem.*, 1984, **23**, 3671–3673.
111 F. Yu and L. Xu, *Dalton Trans.*, 2019, **48**, 17445–17450.
112 B. Luo and L. Xu, *Dalton Trans.*, 2019, **48**, 6892–6898.
113 X. Xu, B. Luo, L.-L. Wang and L. Xu, *Dalton Trans.*, 2018, **47**, 3218–3222.
114 F. Yu, B. Luo, R. Sang and L. Xu, *Nanoscale*, 2020, **12**, 20230–20238.
115 A. E. Dearle, D. J. Cutler, H. W. L. Fraser, S. Sanz, E. Lee, S. Dey, I. F. Diaz-Ortega, G. S. Nichol, H. Nojiri, M. Evangelisti, G. Rajaraman, J. Schnack, L. Cronin and E. K. Brechin, *Angew. Chem., Int. Ed.*, 2019, **58**, 16903–16906.
116 B. Luo, R. Sang, L. Lin and L. Xu, *Catal. Sci. Technol.*, 2019, **9**, 65–69.
117 E. Guillamón, M. Oliva, J. Andrés, R. Llusar, E. Pedrajas, V. S. Safont, A. G. Algarra and M. G. Basallote, *ACS Catal.*, 2021, **11**, 608–614.
118 O. Linnenberg, A. Kondinski and K. Y. Monakhov, in *Supramolecular Systems*, ed. C. Pena, Hauppauge : Nova Science Publishers, 2017, pp. 39–66.
119 J. A. Hollingshead and R. E. McCarley, *J. Am. Chem. Soc.*, 1990, **112**, 7402–7403.
120 A. Flemming and M. Köckerling, *Angew. Chem., Int. Ed.*, 2009, **48**, 2605–2608.
121 X. Yu, A. R. Oganov, I. A. Popov and A. I. Boldyrev, *J. Comput. Chem.*, 2016, **37**, 103–109.
122 W. L. Jolly, *Modern inorganic chemistry*, Mcgraw Hill International Edition, 2017.
123 X. Wei, R. E. Bachman and M. T. Pope, *J. Am. Chem. Soc.*, 1998, **120**, 10248–10253.
124 M. N. Sokolov, I. V. Kalinina, E. V. Peresypkina, N. K. Moroz, D. Y. Naumov and V. P. Fedin, *Eur. J. Inorg. Chem.*, 2013, **2013**, 1772–1779.
125 N. N. Sveshnikov, M. H. Dickman and M. T. Pope, *Inorg. Chim. Acta*, 2006, **359**, 2721–2727.
126 X. Wei, M. H. Dickman and M. T. Pope, *Inorg. Chem.*, 1997, **36**, 130–131.
127 F. A. Cotton and T. R. Felthouse, *Inorg. Chem.*, 1980, **19**, 323–328.
128 M. E. Tess and J. A. Cox, *Electroanalysis*, 1998, **10**, 1237–1240.
129 A. M. Kijak, R. K. Perdue and J. A. Cox, *J. Solid State Electrochem.*, 2004, **8**, 376–380.
130 M. M. Wandstrat and J. A. Cox, *Electroanalysis*, 2007, **19**, 49–54.
131 K. M. Wiaderek and J. A. Cox, *Electrochim. Acta*, 2011, **56**, 3537–3542.
132 M. N. Sokolov, V. S. Korenev, N. V. Izarova, E. V. Peresypkina, C. Vicent and V. P. Fedin, *Inorg. Chem.*, 2009, **48**, 1805–1807.
133 C.-G. Liu, *Mol. Phys.*, 2011, **109**, 1851–1857.
134 J. Martin-Frere and Y. Jeannin, *Inorg. Chem.*, 1984, **23**, 3394–3398.
135 H. Schmidbaur and A. Schier, *Organometallics*, 2015, **34**, 2048–2066.
136 W. H. Knoth Jr., *Obituary from 9 April 2008*, The News Journal, Wilmington Del., USA, 2008, 16.
137 P. J. Domaille and W. H. Knoth, *Inorg. Chem.*, 1983, **22**, 818–822.
138 W. H. Knoth, P. J. Domaille and R. D. Farlee, *Organometallics*, 1985, **4**, 62–68.
139 R. Cao, K. P. O'Halloran, D. A. Hillesheim, S. Lense, K. I. Hardcastle and C. L. Hill, *CrystEngComm*, 2011, **13**, 738–740.
140 G. Sazani, M. H. Dickman and M. T. Pope, *Inorg. Chem.*, 2000, **39**, 939–943.
141 S. Reinoso, M. H. Dickman, A. Praetorius, L. F. Piedra-Garza and U. Kortz, *Inorg. Chem.*, 2008, **47**, 8798–8806.
142 N. Seriani, W. Pompe and L. C. Ciacchi, *J. Phys. Chem. B*, 2006, **110**, 14860–14869.
143 M. Girardi, D. Platzer, S. Griveau, F. Bedioui, S. Alves, A. Proust and S. Blanchard, *Eur. J. Inorg. Chem.*, 2019, **2019**, 387–393.
144 P. Yang, Y. Xiang, Z. Lin, Z. Lang, P. Jiménez-Lozano, J. J. Carbó, J. M. Poblet, L. Fan, C. Hu and U. Kortz, *Angew. Chem., Int. Ed.*, 2016, **55**, 15766–15770.
145 J. Yang and R. Jin, *ACS Mater. Lett.*, 2019, **1**, 482–489.
146 R. Jin, C. Zeng, M. Zhou and Y. Chen, *Chem. Rev.*, 2016, **116**, 10346–10413.
147 Y. Kikukawa, Y. Kuroda, K. Suzuki, M. Hibino, K. Yamaguchi and N. Mizuno, *Chem. Commun.*, 2013, **49**, 376–378.
148 K. Yonesato, H. Ito, D. Yokogawa, K. Yamaguchi and K. Suzuki, *Angew. Chem.*, 2020, **59**, 16361–16365.
149 K. Yonesato, H. Ito, H. Itakura, D. Yokogawa, T. Kikuchi, N. Mizuno, K. Yamaguchi and K. Suzuki, *J. Am. Chem. Soc.*, 2019, **141**, 19550–19554.
150 Y. Zhang, L. Li, T. Sun, B. Liu, H. Hu and G. Xue, *Inorg. Chem.*, 2011, **50**, 2613–2618.
151 G. Savelsberg and H. Schäfer, *Z. Naturforsch., B: Anorg. Chem., Org. Chem.*, 1979, **34**, 1033–1034.
152 S. Duval, M.-A. Pilette, J. Marrot, C. Simonnet-Jégat, M. Sokolov and E. Cadot, *Chem. – Eur. J.*, 2008, **14**, 3457–3466.
153 S. Duval, J. Marrot, C. Simonnet-Jégat, I. M. Mbomekallé, M. Sokolov and E. Cadot, *Dalton Trans.*, 2012, **41**, 3174–3184.
154 M. Shibasaki, H. Sasai and T. Arai, *Angew. Chem., Int. Ed. Engl.*, 1997, **36**, 1236–1256.
155 B. G. Cooper, J. W. Napoline and C. M. Thomas, *Catal. Rev.*, 2012, **54**, 1–40.

